TURBULENT HEAT TRANSFER IN A TRAPEZOIDAL CHANNEL WITH TRANSVERSE AND V-SHAPED RIBS ON TWO OPPOSITE WALLS

A Thesis

by

KARTHIK SUBRAMANIAN

Submitted to the Office of Graduate Studies of
Texas A&M University
in partial fulfillment of the requirements for the degree of

MASTER OF SCIENCE

December 2005

Major Subject: Mechanical Engineering

TURBULENT HEAT TRANSFER IN A TRAPEZOIDAL CHANNEL WITH TRANSVERSE AND V-SHAPED RIBS ON TWO OPPOSITE WALLS

A Thesis

by

KARTHIK SUBRAMANIAN

Submitted to the Office of Graduate Studies of
Texas A&M University
in partial fulfillment of the requirements for the degree of

MASTER OF SCIENCE

Approved by:

Chair of Committee,	Sai Lau
Committee Members,	Nagamangala K.Anand
	Yassin A.Hassan
Head of Department,	Dennis O'Neal

December 2005

Major Subject: Mechanical Engineering

ABSTRACT

Turbulent Heat Transfer in a Trapezoidal Channel with Transverse and V-shaped Ribs on Two Opposite Walls. (December 2005)

Karthik Subramanian, B.E., University of Madras

Chair of Advisory Committee: Dr. Sai Lau

This study investigates the turbulent heat transfer and friction in a trapezoidal channel with opposite walls roughened with transverse and v-shaped ribs. The roughened channel depicts the internal cooling passage of an aerofoil near the trailing edge. The various configurations investigated for this study are smooth channel, channel with 90° transverse ribs and channel with v-shaped ribs angled at 45°. The pitch-to-height ratio (P/e), rib height-to-hydraulic diameter ratio ($e/D_{h)}$ and the aspect ratio (W/e) were maintained at 12, 0.1906 and 1, respectively. The configuration was tested for Reynolds number ranging from 7,000 to 40,000. The 45° rib was found to produce the maximum heat transfer and minimum pressure loss.

TO

MY GRANDPARENTS & PARENTS

ACKNOWLEDGEMENTS

I would like to thank the chair of my committee, Dr Sai Lau, for all his help, support, time and effort, without which this work would not have been possible. His ideas and valuable input were vital to the successful completion of my work. I would also like to take this opportunity to thank my committee members, Dr N.K. Anand and Dr Yassin A.Hassan, whose cooperation and assistance were valuable to the completion of this project within the stipulated time.

I would also like to thank the heat transfer lab technician, Ysidoro Ramirez for his time and dedication in helping me procure in a timely manner all the materials, instruments, etc. needed for my research. My acknowledgments would be incomplete without mentioning the help rendered by Mike Walker, the workshop technician.

Last, but not least, I would like to thank my lab mates and my friends whose support has been instrumental in the successful completion of my project.

NOMENCLATURE

A	heat transfer surface area
B	bias limit
C_p	specific heat at constant pressure
D_h	hydraulic diameter
d_o	diameter of orifice
e	rib height
f	friction factor
f_o	friction factor in fully developed tube flow
H	Heat transfer coefficient
I	current input
K	thermal conductivity of air
l	plenum length
L	length of slab
$\dot{m}$	mass flow rate
Nu	Nusselt number
$\overline{Nu}$	Average Nusselt number
Nu_o	Nusselt Number in fully developed tube flow
Δp	pressure drop across test section
P	rib pitch
p_o	pressure upstream of orifice

P_w	wetted perimeter
P_x	random error
Pr	prandtl number
$\dot{q}$	heat flux
Re	Reynolds number
S_x	precision index
t(N,C)	confidence level
T_i	temperature of slab
T_b	bulk mean temperature
T_w	local wall temperature
U_x	relative uncertainty of x
V	voltage input
W	flow channel width
W/H	channel aspect ratio

Constants (calculated)

C	discharge coefficient
Y	expansion coefficient

Greek symbols

α	rib angle-of-attack
σ	standard deviation

μ	average dynamic viscosity of air
ρ	average density of air

TABLE OF CONTENTS

Page

LIST OF FIGURES

FIGURE Page

LIST OF TABLES

INTRODUCTION

Gas turbines, as a prime mover, find a wide range of applications in the industrial world today. Therefore, it is important to develop highly efficient gas turbines using the latest state-of-the-art technologies. One of the traditional methods used to improve the efficiency of a gas turbine is to increases the inlet temperature; thereby increasing the power output and, in turn, the efficiency.

The problem associated with increasing the inlet temperature of a gas turbine is the failure of material due to excessive thermal stresses. This brings in the concept of cooling of turbine blades to incorporate the increase in the inlet temperature. The cooling should be optimized, as lack of cooling will cause failure of material and excess cooling will cause a decrease in efficiency of the turbine.

The two main methods of cooling are internal and external cooling. The three main internal cooling methods are namely jet impingement cooling, rib-turbulated cooling and end cooling. The main focus of this research is rib-turbulated cooling.

Fig. 1 shows the cooling methodology in a typical blade of a gas turbine, which is cooled mainly by convection. The turbine consists of internal passages, which are serpentine. The passage near the trailing edge of the blade consists of pin fins so as to enhance the heat transfer rate. Part of air is ejected out through small holes near the leading edge, which is used for film cooling on the outer blade surface. This ejected cool air forms a thin film over the surface, there by, insulating it from the hot gases.

This thesis follows the style of *Journal of Heat Transfer.*

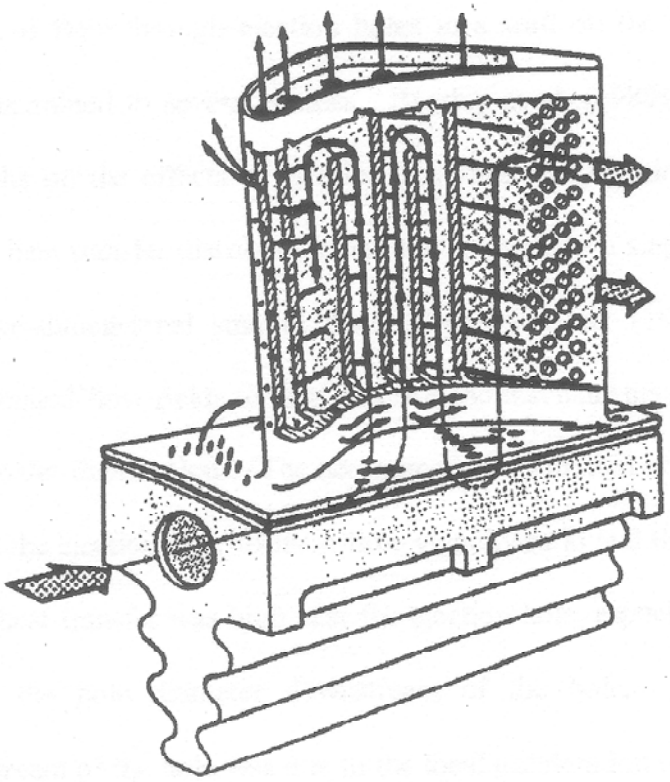

Fig. 1 Gas Turbine Cooling Methodology

Jet impingement cooling is one of the most effective ways of internal cooling as high heat transfer coefficients can be achieved. Therefore the jet impingement cooling is mostly used near the leading edge of the airfoil where the thermal loads are high. Also the thicker cross section near the leading edge makes the housing of nozzle easier. Jet impingement cooling is not preferred at the mid-chord section of the rotor blade as the arrangement reduces the structural strength of the blade; however it is used in the mid-chord section of the stator blade.

The trailing edge of the blade is usually cooled using pin fins. The fins are arranged in such a manner that they block the flow, which results in forced convected fin cooling. These fins help in two different ways to enhance the heat transfer. Firstly, they introduce wakes into the stream thereby creating free stream turbulence. These wakes not only disturb the flow but also enhance the heat transfer from the fins down-stream. Secondly, the pin fins help in increasing the effective heat transfer area there by helping in effective removal from the surface.

The internal passages in the mid-rib section of the airfoil usually have either a rectangular cross section or a trapezoidal cross section. These passages are usually roughened with ribs on two opposite walls that are exposed to hot combustion gases on the outside, so as to augment the heat transfer from the blade to the cooling air. These ribs causes flow separation. In some cases secondary flows cause turbulent mixing near the wall where these flow separations reattach the boundary layer to the wall.

The current research is aimed at studying the streamwise variation of the regional average heat transfer coefficient, along a duct, trapezoidal in cross-section, which

models the internal cooling passage of an airfoil. The study will be conducted with three channels: one with smooth walls, one with 90° transverse ribs on two opposite walls and one with 45° V-shaped ribs on two opposite walls, for Reynolds number varying between 8,000 and 40,000 as shown in Fig. 2. The pitch-to-height (*P*/*e)* ratio will be maintained at 12 and the rib height at about 10% of the hydraulic diameter.

The Nusselt number, which is a dimensionless heat transfer coefficient, will be normalized with the Nusselt number for the fully developed turbulent flow in a smooth channel, calculated with a correlation by McAdama/Dittus-Boelter to study the heat transfer augmentation.

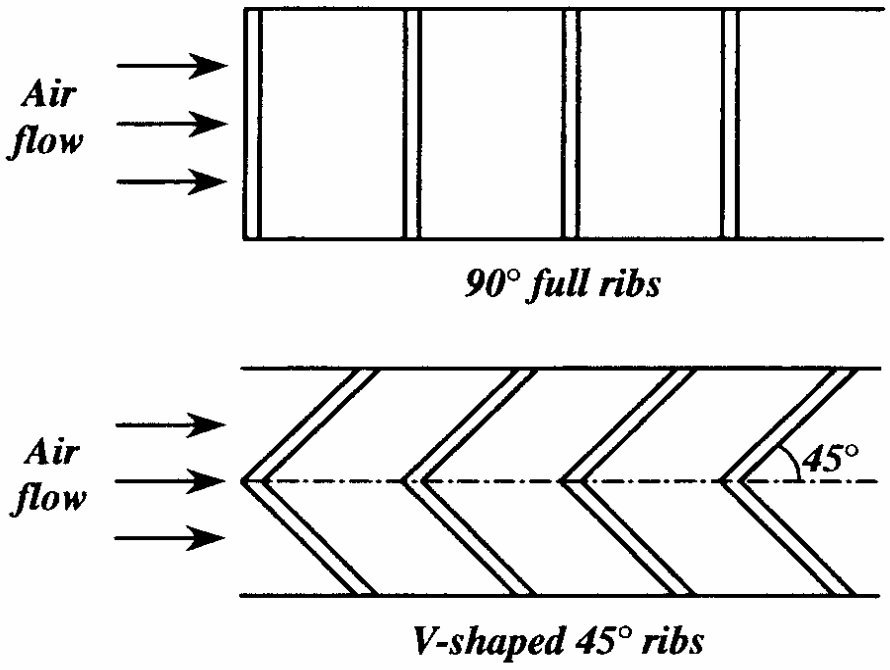

Fig. 2 Rib Configuration Examined

LITERATURE REVIEW

Review of Previous Work

Extensive research has been conducted in the field of turbulated cooling both experimentally and numerically. The research focuses have been on channels with square, rectangular, and triangular cross sections, and with either single pass or multiple passes. The heat transfer coefficients have been studied for various rib configurations, Reynolds numbers, aspect ratios (*W*/*H*), and pitch-to-height (*P*/*e)* ratios. Procedures adopted for studying heat transfer coefficient have included both steady state heat transfer experiments and mass transfer experiments using mass-heat transfer analogy.

The effect of Prandtl number on heat transfer and friction in smooth and rough tubes was studied by Dippery et al. [1]. The results showed that the heat transfer increased by a factor to 2-3 when rough tubes replaced smooth tubes at the expense of increase in friction. However at high Prandtl number the improvement in heat transfer was achieved without any loses by roughening.

Han et al. [2] investigated the heat transfer and friction characteristics of rib roughened surfaces for various angle of attacks, rib profiles and *P*/*e* ratios. It was found that ribs placed at an angle of attack of 45° had superior heat transfer performance for a given friction power when compared to that of ribs at an angle of attack of 90°. Also it was once again concluded that the heat transfer and friction was maximum for a *P*/*e* ratio of 10.

Han [3] studied the heat transfer and friction in square channel with opposite rib-roughened wall for Reynolds number ranging from 7,000 to 90,000. The Staton number at the ribbed wall was found to be 1.5 to 2.2 times than that of the four-sided smooth duct. The average friction factor also was found to increase by a factor of 2.1 to 6.

The variation of pressure drop and average heat transfer along a square duct for Reynolds number ranging from 7,000 to 90,000, P/e ratio varying from 10 to 20 and for various rib configuration was studied by Han et al. [4]. The results showed that for (α = 90°) the average Nusselt number was twice the average Nusselt number for a smooth channel and the friction factor increase about four to six times. The heat transfer enhancement was found to be better for (α = 45° and 30°) in comparison to other configuration. The heat transfer for (α = 45°) was found to be twenty five times greater than that for (α = 90°) but the friction factors remained the same. The 45° angled ribs were found to consume 20-50% less pump power when compared to 90° straight ribs. Also the pump power required for P/e = 10 was found to be less than for P/e = 20. In general the angled ribs were found to provide better cooling effect than the 90° straight ribs and P/e ratio of 10 was found to be advantageous than P/e ratio of 20.

The internal cooling passage near the leading edge of the airfoil is usually triangular in cross section. Therefore Metzger et al. [5] and Luo [6] investigated the heat transfer in triangular channels with angled roughness ribs on two walls. It was once more proven that the V-shaped ribs produced higher heat transfer augmentation than the 90° transverse rib due to the stream-wise growing cross-channel secondary flow induced by the angled ribs. The 60° V-shaped ribs resulted in higher heat transfer than the 30° ribs

and the optimum *P*/*e* ratio was found to be around 7.5. The study revealed that the heat transfer coefficient reached a maximum along the test channel and finally decreased towards the end of the channel due to the reflection of the secondary flow thus affecting the flow pattern. It was concluded that the heat transfer augmentation in triangular channel with ribs, was higher than that in square channel with ribs.

Han et al. [7] investigated the developing heat transfer in rectangular channels with rib turbulators for rib angle varying from 90° to 30°. The combined effects of rib angle and channel aspect ratio on local heat transfer coefficient were studied. The results indicate that the best heat transfer in square channel was obtained with angled ribs at 30-45° and was about 30% higher than the 90° transverse ribs for constant pumping power. However, for rectangular channel with aspect ratio of 2 and 4, the heat transfer enhancement using 30°-45° ribs was only 5% more than the 90° transverse rib. In general, it was noted that in square channel the heat transfer increased with decrease in rib angle whereas in rectangular channel the dependence of heat transfer on rib angle was negligible.

Han [8] investigated the heat transfer and friction characteristics in rectangular channel with rib turbulator. The distribution of local heat transfer coefficient was studied for varying channel aspect ratio at various Reynolds numbers raging from 10,000-60,000. The rib angle of attack was maintained at 90° and the experiment was conducted for two *P*/*e* ratios of 10 and 20. The result suggests that the local Nusselt number becomes uniformly periodic between the ribs. The local Nusselt number was found to increase by a factor of 2-3 for various ribbed configuration in comparison to the smooth

channel. The local Nusselt number was found to decrease with increase in spacing and Reynolds number and found to increase with increase in rib height and aspect ratio for a given Reynolds number. The heat transfer augmentation was found to be higher for smaller aspect ratio for a given pumping power.

Lau et al. [9] studied the turbulent heat transfer and friction in square channel with discrete rib turbulators for Reynolds number ranging from 10,000 to 80,000. The studies revealed that the heat transfer in 90° discrete ribs were 10-15% higher than that of the 90° transverse ribs. The overall thermal performance of oblique ribs at (α = 60°, 45° and 30°) was found to be 20% more than that of 90° discrete ribs. Also the crossed oblique ribs were found to have poor thermal performance and so are not recommended for internal cooling of gas turbines.

The effect of rib configuration and Reynolds number on the local heat transfer distribution and pressure drop in a square channel with two opposite in-lined ribbed walls was studied by Han et al. [10]. The results show that for the various rib configurations the Nusselt number ratio decreases with increase in axial distance and attains a constant value downstream. The studies also indicate that for V-shaped ribs the heat transfer augmentation was higher in comparison with other configurations and the reversed V-shaped ribs produced the maximum pressure drop. The heat transfer performance was found to decrease with increase in Reynolds number.

The effect of V-shaped rib arrays on turbulent heat transfer and friction of fully developed flow in a square channel was studied by Lau et al. [11]. The configuration investigated included V-shaped ribs angled at 45°, 60°, 90°, 120° and 135° for a P/e

ratio of 10.The results indicated that the V-shaped ribs at (α = 46° and 60°) produced a 38%-46% and 47%-66% increase in thermal performance when compared to the 90° full rib. Similarly, when the following ribs were reversed, the heat transfer performance was enhanced by 26%-32% and 39%-48% respectively. This enhancement in thermal performance was accompanied by a 55%-79% increase in the pressure drop for various V-shaped configurations in comparison to the 90° rib. The reversed V-shaped ribs was found to result in poor heat transfer performance. The crossed ribs whose performance was also investigated resulted in poor heat removal. It was also found that doubling the P/e ratio lowers the heat transfer augmentation and friction.

Liou [12] investigated the turbulent heat transfer augmentation and friction in periodic fully developed channel flow using laser holographic interferometer and thermocouples. The distribution of average friction factor as well as the average and local Nusselt was studied for Reynolds number varying from 5,000 to 54,000, the P/e ratio of 10, 15 and 20 and e/D_h ratios of 0.063, 0.081 and 0.106. The results showed that there was 2.2 to 17 fold increase in the average Nusselt number for various e/D_h ratios and Reynolds number. The heat transfer augmentation was found to increase with increase in e/D_h ratios. The ribs were found to transfer more heat than the duct wall does on a unit area basis. The results proved that the heat transfer decreases with the increase spacing between the ribs. The rate of increase in Nusselt number with Reynolds number is less for the ribbed duct in comparison to the smooth duct, which results in the decrease in the Nusselt number ratio with increase in Reynolds number. The reason attributed to this behavior is that a fraction of the mean flow energy is converted into turbulent kinetic

energy in the ribbed duct, which subsequently results in enhancement of heat transfer through turbulent transport.

The influence of surface heat flux on heat transfers augmentation in square channels with parallel, crossed and V-shaped angles ribs were studied by Han et al. [13]. The test was conducted on square channel with L/D ratio of 20, e/D ratio of 0.0625, P/e ratio of 10 and Reynolds number ranging from 15,000 to 80,000. It was found that the ribbed wall heat transfer coefficient increased with increase in the ratio of ribbed side to smooth side wall flux. It also showed that two ribbed side wall heating provided a higher ribbed side wall heat transfer augmentation than the four wall uniform heating. The effect of wall flux ratio was found to reduce with increasing Reynolds number. The results indicate that the 60° v –shaped and parallel ribs performed better that 60° crossed rib and 90° rib irrespective of the wall heat flux ratio and Reynolds number.

Taslim et al. [14] studied the effects of turbulator profile and spacing on heat transfer and friction in a channel with traverse ribs. It was concluded that the heat transfer coefficient was higher for aspect ratios greater than unity but resulted in higher pressure loss. The trapezoidal shaped ribs spaced properly were found to be effective in heat removal. The optimum pitch to height ratio for the 90° square turbulator was found to be around 8. The sensitivity of Nusselt number was found to decrease with decrease in the blockage ratio (e/D_h).

Taslim et al. [15] experimentally investigated the heat transfer and friction in channel roughened with angled V-shaped and discrete ribs on two opposite walls for Reynolds number raging from 5,000 to 30,000. The results showed that the 90°

transverse ribs produced the lowest heat transfer performance. The 45° angled V-shaped ribs produced the highest heat transfer performance in comparison to other rib configurations. For V-shaped ribs facing downstream of flow, the one with lowest blockage ratio had better heat removal rate. The discrete ribs also produced better performance in comparison to the transverse ribs.

Katoh et al. [16] investigated the heat transfer enhancement and pressure loss by surface roughness in turbulent channel flows. The objective of the study was to investigate the relationship between the heat transfer enhancement and the increase in drag by the rough surface using time-space averaged momentum and energy equation. It was concluded that the efficiency of the heat transfer surface in general was less than unity when the molecular Prandtl number of the working fluid is less than the turbulent Prandtl number and vice versa. For fluids with low Prandtl number the drag increase is usually greater than the heat transfer augmentation; however for liquids with higher Prandtl number the eddy viscosity over the rough surfaces has a significant effect on the heat transfer enhancement. This increase in efficiency of the heat transfer surface is true only for smaller roughness elements and for higher roughness elements the efficiency does not normally exceed unity.

Ekkad et al. [17] and Murata et al. [18] studied the heat transfer measurements inside straight and tapered two-pass channel with turbulator ribs as in reality the internal cooling passage has a decreasing cross sectional are from the hub to the tip. The study was conducted for various Reynolds numbers with and without ribs for both straight and tapered channel. The results indicate that at low Reynolds number the heat transfer

augmentation in the first pass in the straight channel is comparable to that of the tapered channel. However, at higher Reynolds numbers, the acceleration effect in the tapered channel results in higher Nusselt number ratios when compared to the straight channel. The tapered channel with ribs, enhanced the heat transfer by a factor of 1.5-2.0 when compared to the tapered smooth channel but in the after-turn region the Nusselt number ratios were found to be comparable. The tapered ribbed channel and straight ribbed channel was found to provide similar augmentation level in most of the channel.

Heat transfer and friction behaviors in rectangular channel with varying number of ribbed walls were investigated by Chandra et al. [19]. The test was performed with ribs on one, two, three and four walls for Reynolds number ranging from 10,000 to 80,000. The P/e and e/D_h ratios were maintained at 8 and 0.0625, respectively. It was clear, by the results, that the heat transfer enhancement increased with increase in the number of ribbed walls due to increase in turbulence. The Nusselt number ratio was found to decrease along the streamwise direction and remains a constant once the flow becomes fully developed. The Nusselt number ratio also decreased with increase in Reynolds number. The heat transfer enhancement for the two-sided ribbed wall was found to be in the range of 2.64 to 1.92. It was also noted that the friction factor ratio increased with increase Reynolds number. The heat transfer performance was studied and the results indicate a significant decrease in the performance with increase in the number of ribbed walls and Reynolds number.

Objective

As stated earlier, with the invention of high efficiency gas turbine engines, there is a need to effectively cool the turbine blades to prevent the failure of material due to excess heating by the high-temperature combustion gases flowing over the exterior surfaces of the blades. Most of the studies carried out thus far by researchers have been conducted on channels that had square, rectangular, or triangular cross sections. The actual passages in the airfoil are all not exactly rectangular in cross section. In fact, most of these passages are trapezoidal in cross section as shown in Fig. 3. So, the need arises to study the heat transfer coefficient distribution along a trapezoidal channel for various rib configurations and flow rates.

The objective of this research is to determine the streamwise variation of the regional average heat transfer coefficient along a smooth trapezoidal channel and two channel of the same trapezoidal cross section with 90° transverse ribs and 45° V-shaped ribs on two opposite walls. The Nusslet number, which is a dimensionless heat transfer coefficient, will be normalized with the Nusselt number for the fully developed turbulent flow in a smooth channel, calculated with a correlation by McAdama/Dittus-Boelter to study the heat transfer augmentation.

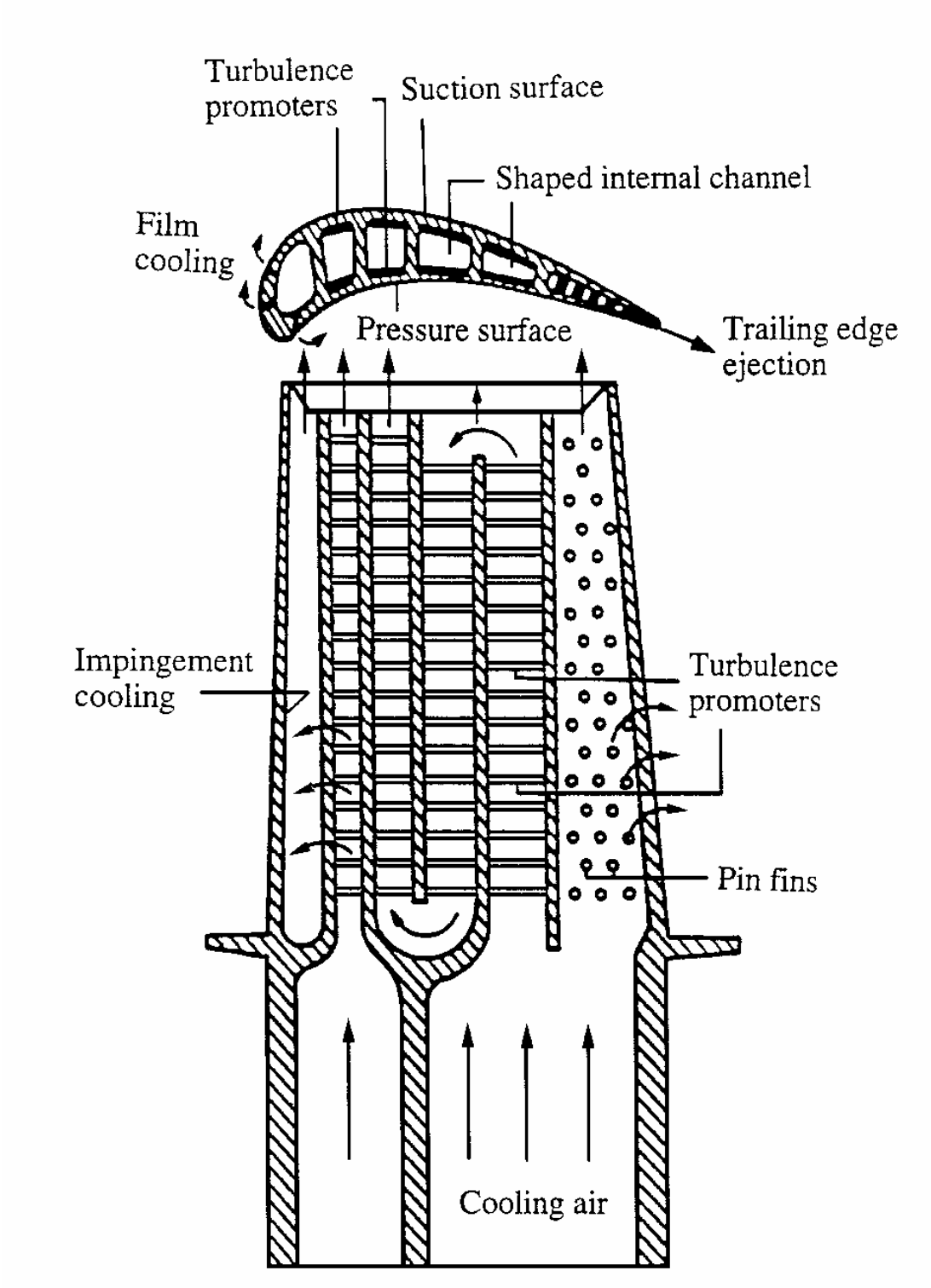

Fig. 3 Cooling Concept in Modern Turbine Blade

EXPERIMENTAL ANALYSIS

Rib Turbulated Cooling Theory

The rib turbulated cooling is one of the most common methods used in the mid rib section of a blade. In rib turbulated cooling, ribs are cast on two opposite walls usually on the walls of the suction and pressure sides of the aerofoil. These turbulent promoters help in transferring the heat effectively from the blade to the flowing air, thereby enhancing the cooling process. Researchers have found that parameters that mainly influence the heat transfer are the Reynolds number, the channel aspect ratio (W/H), blockage ratio (e/D_h) and the rib configurations. In general, the pitch to rib height ratio (P/e) and blockage ratio e/D_h are selected in the ranges of 7 to 15 and 5% to 10% respectively, so as to optimize the heat transfer augmentation and pressure drop losses.

The flow, past the turbulent promoters cast on the walls of the passages are characterized by boundary layer separations and are followed by reattachment of the boundary layer to the heat transfer surface, which results in the enhancement of the heat transfer coefficient. The schematic representation of the rib on the wall and the flow separation near the rib are shown in Fig. 4**.**

The separation occurs at the ribs, which lead to the formation of a shear layer and finally reattaches at about 6-8 times the rib height, downstream of the rib. The reverse flow boundary was found to originate from the reattachment point and had grown in thickness. The wall shear stress is zero at the reattachment point and was found to

increase in the reverse flow region. Research by Webb [20] has shown that reattachment does not take place below a particular *P*/*e* ratio.

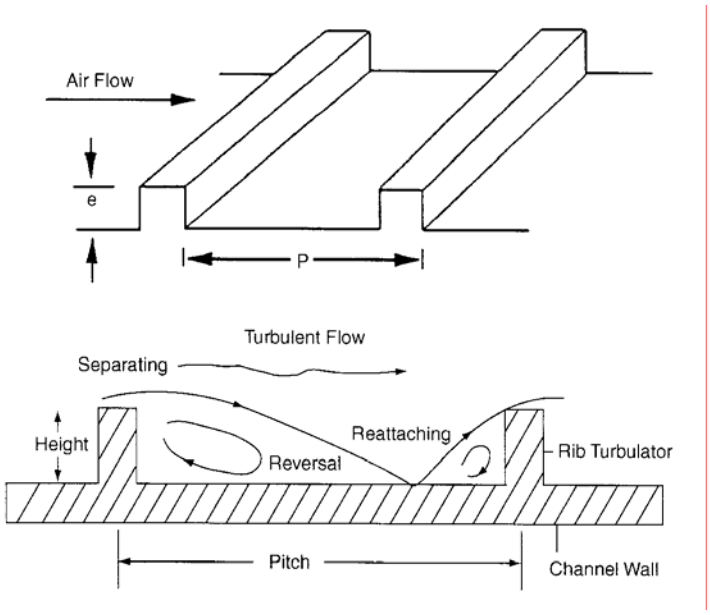

Fig. 4 Flow Separation on the Ribs

Various researchers have studied the effects of ribs and the results have been discussed previously. The secondary flow produced by V-shaped ribs is shown in Fig. 5**.**

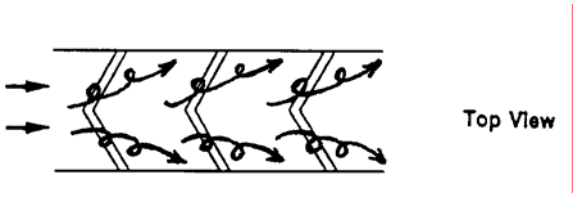

Fig. 5 Cross Stream Secondary Flows Induced by V-shaped Ribs

These flows induce turbulent mixing which result in effective transfer of heat from the walls to the flowing fluid because of the increase in heat transfer coefficient. However, increase in the heat transfer augmentation is accompanied by pressure drop penalty.

Methodology

To study the heat transfer coefficient distribution along the internal passage of an aerofoil, a test section was constructed. The test section is 137.16 cm (54 in.) in length with a trapezoidal cross section whose parallel walls are 3.81 cm (1.5 in.) and 11.43 (4.5 in.) wide, and the other walls are 7.62 cm (3 in.) and 10.78 cm (4.2426 in.) wide, respectively as shown in Fig. 6. The first 60.96 cm (24 in.) of the test channel is used for developing a flow and the last 15.24 cm (6 in.) connects to the settling plenum. The remaining 60.96 cm (24 in.) in the middle is the actual test section with the parallel walls made of wood and the other walls made of aluminum wall segments.

One of the two aluminum wall is oriented at an angle of 45^{o} with respect to the other. One of these walls is made of 16 identical aluminum wall segments of dimension 7.46 cm x 3.73 cm x 1.27 cm (2.938 in. x 1.469 in. x 0.5 in.). These wall segments are separated by balsa wood strips of thickness 0.159 cm (0.0625 in.) arranged in an array of 2 by 8. The opposite wall is again made of 16 identical aluminum wall segments but, of dimension 7.46 cm x 5.31 cm x 1.27 cm (2.938 in. x 2.09 in. x 0.5 in.) separated by balsa wood and arranged in a similar fashion. The balsa strips are glued to the wall segments

using silicon gel II to prevent conduction of heat from one wall segment to the other as shown in Fig. 7.

Two heaters are glued to the backside of the aluminum arrays to provide a uniform heat flux, which is used as heat input to the test section. The heat input to the two heaters was controlled independently by two variable transformers. Two thermocouples were installed in each wall segment to measure the average temperature of the wall segment. Holes of appropriate diameters were drilled at various locations and the thermocouples were inserted into the holes and glued using 5 min epoxy.

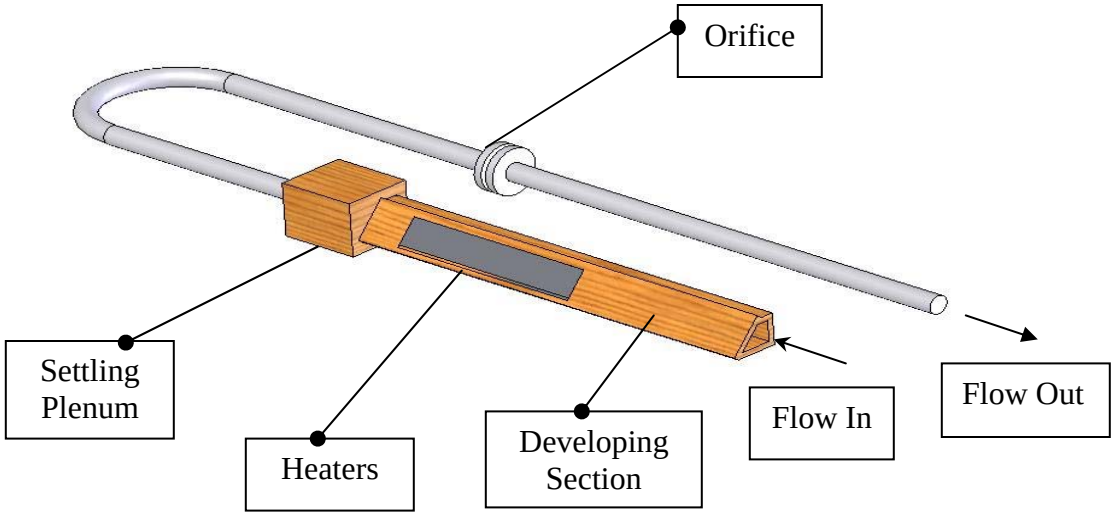

Fig. 6 Schematic of Teat Apparatus for Average Heat Transfer Measurement

The exit of the channel is connected to a settling plenum. An orifice is attached to the pipe to measure the flow rate through the channel. Pressure taps were installed across the test section and across the orifice to measure the respective pressure drop.

Fig. 7 Schematic of Test Section with V-shaped Ribs

Three additional thermocouples were installed to measure the temperature of air entering the channel, the exit air temperature, and the air temperature, immediately downstream

of the orifice. The output of all the thermocouple was recorded with a computer-controlled data acquisition system that uses hardware and LabView software from National Instruments, Inc.

The pressure drop across the orifice was measured with an inclined manometer and the drop across the test section was measured with micromanometer. The voltage and current are measured with a multimeter and an ammeter, respectively, product of which gives the power supplied to the two heaters and, in turn, the heat flux supplied to the test section.

The ribs used for various cases are made of aluminum with dimensions 6.35 mm x 6.35 mm (0.25 in. x 0.25 in.). The pitch-to-height ratio was maintained at 12 and the height of the rib was approximately 9.25% of the channel hydraulic diameter. The ribs were machined to the required dimensions and angles and were glued to the slab at the required locations as shown in Fig. 8. The thickness of the glue was kept to a minimum so as to reduce the thermal resistance offered to the flow of heat.

A centrifugal pump of power 1.5 Hp was used to force the required amount of air through the duct and the exhaust from the pump was forced out through the hood. The pump was operated at two different speeds depending on the mass flow rate required. For safe operation of the pump at low Reynolds number a bypass valve is used to feed in air.

The experiment was run for 5 different Reynolds numbers ranging from 8,000 to 40,000. The variable transformers were adjusted in such a way that equal flux was

supplied through the aluminum wall segments and the average steady state temperature was maintained at around 30° over the ambient temperature so as to minimize the error.

The test section of model was insulated with fiberglass and other insulating material in order to minimize heat loss to the surrounding. Heat loss experiments were carried out in plugged flow condition, in order to evaluate the percentage heat loss to the ambience.

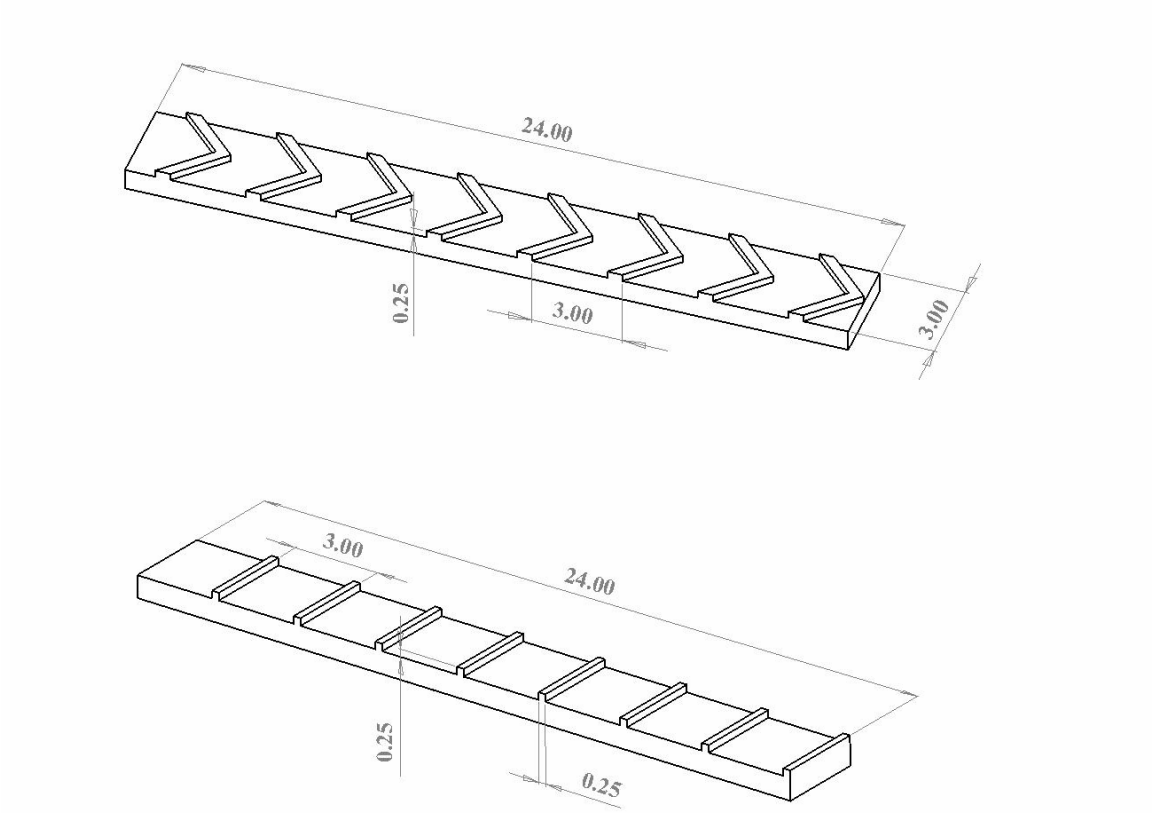

Fig. 8 Rib Orientation

The values of the average heat transfer coefficient and Nusselt numbers were calculated by reducing the data obtained and the results presented graphically and in tables are analyzed.

Data Reduction

The heat transfer coefficient for the "i" wall segment was calculated using the net heat input to the wall; the wall temperature and the bulk mean temperature as

$$h_i = \frac{q_i}{A_{s,i}(\overline{T}_{w,i} - \overline{T}_{b,i})} \tag{3.1}$$

The actual heat going into the duct is given by the amount of power supplied which is the product of voltage applied and the current flowing in the circuit minus the amount of heat loss from each plate. The flexible heaters were assumed to supply uniform heat to all the slabs. The heat loss from the test section to the surrounding was calculated experimentally by conducting a no-flow condition. The heat loss to the surrounding was found to vary between 5-15% for various Reynolds number. The major heat loss was found to occur through the thick wired copper thermocouples installed in each wall segment.

The Nusselt number was normalized using the Nusselt number correlation for a fully developed flow in a smooth circular channel. The relative uncertainty on Nusselt number was found to be 5%.

$$\frac{Nu}{Nu_o} = \left(hD_h/k\right) / \left[0.023Re^{0.8}Pr^{0.4}\right] \tag{3.2}$$

All the temperatures were measured using the thermocouples. The bulk mean air temperature at the inlet and the exit was measured using the thermocouples and the bulk mean temperature at the end of each plate was calculated using the formula given by

$$T_{b,out} = T_{b,in} + \frac{q}{\dot{m}c_p} \tag{3.3}$$

The pressure drop measured with a micromanometer across the test section, was used to calculate the friction factor. The relation between pressure drop and friction factor is given by

$$f = \frac{\left(\frac{\Delta p}{\Delta x}\right) D_h}{\frac{\rho \bar{u}^2}{2}} = 2\rho \left(\frac{\Delta p}{\Delta x}\right) D_h \left(\frac{A_c}{\dot{m}}\right)^2 \tag{3.4}$$

The fiction factor is normalized by Gnielinski equation

$$f_o = \left[0.79 \ln(Re_{Dh}) - 1.64\right]^{-2} \tag{3.5}$$

The correlation for thermal performance is given by

$$TP = (\overline{Nu}/Nu_o)/(\overline{f}/f_o)^{1/3} \tag{3.6}$$

RESULT AND DISCUSSION

Heat Transfer Distribution in Smooth Channel

The average heat transfer results for a smooth channel at four different walls are represented as the streamwise distribution of a normalized Nusselt number in Figs. 10-13. The Nusselt number was normalized with the Nusselt number for fully developed turbulent flow in smooth circular tube correlated by McAdams/Dittus-boelter. The Nusselt number ratios at all four cases was found to decrease with increasing axial distance and finally reaches a constant value where, normalized axial distance X/D_h is greater than four and the flow becomes fully developed for a given Reynolds number.

The maximum uncertainty in the Nusselt number ratios was found to be 5% and the deviation of the Nusselt Number from the McAdams/Dittus Boelter correlation was found to be 15%-20% for the smooth channel. The average Nusselt number was calculated as a mean of Nusselt numbers corresponding to values of X/D_h between 2.2 and 7.7, corresponding to the developed region.

The Nusselt number was found to increase on all the four walls with increasing Reynolds number. The reason attributed to this behavior is as Reynolds number increases the turbulent mixing is enhanced in the channel which leads to effective removal of heat. However, the Nusselt number ratio which is obtained by normalizing the average Nusselt number with the fully developed turbulent flow in smooth circular tubes correlated by McAdams/Dittus Boelter was found to decrease as shown in Fig. 14.

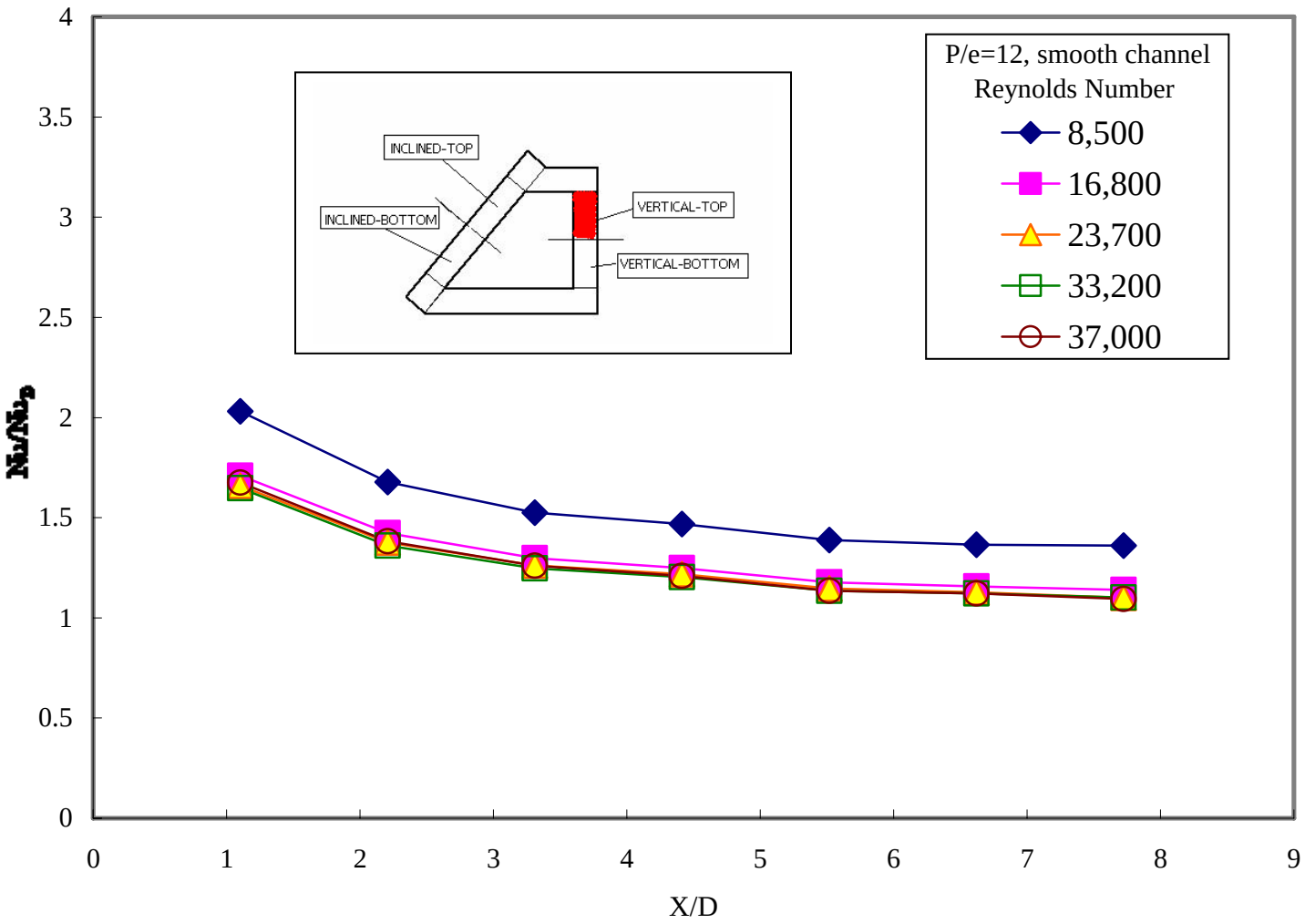

Fig. 10 Effect of Reynolds Number on Heat Transfer Distribution on Vert-Top Wall in Smooth Channel

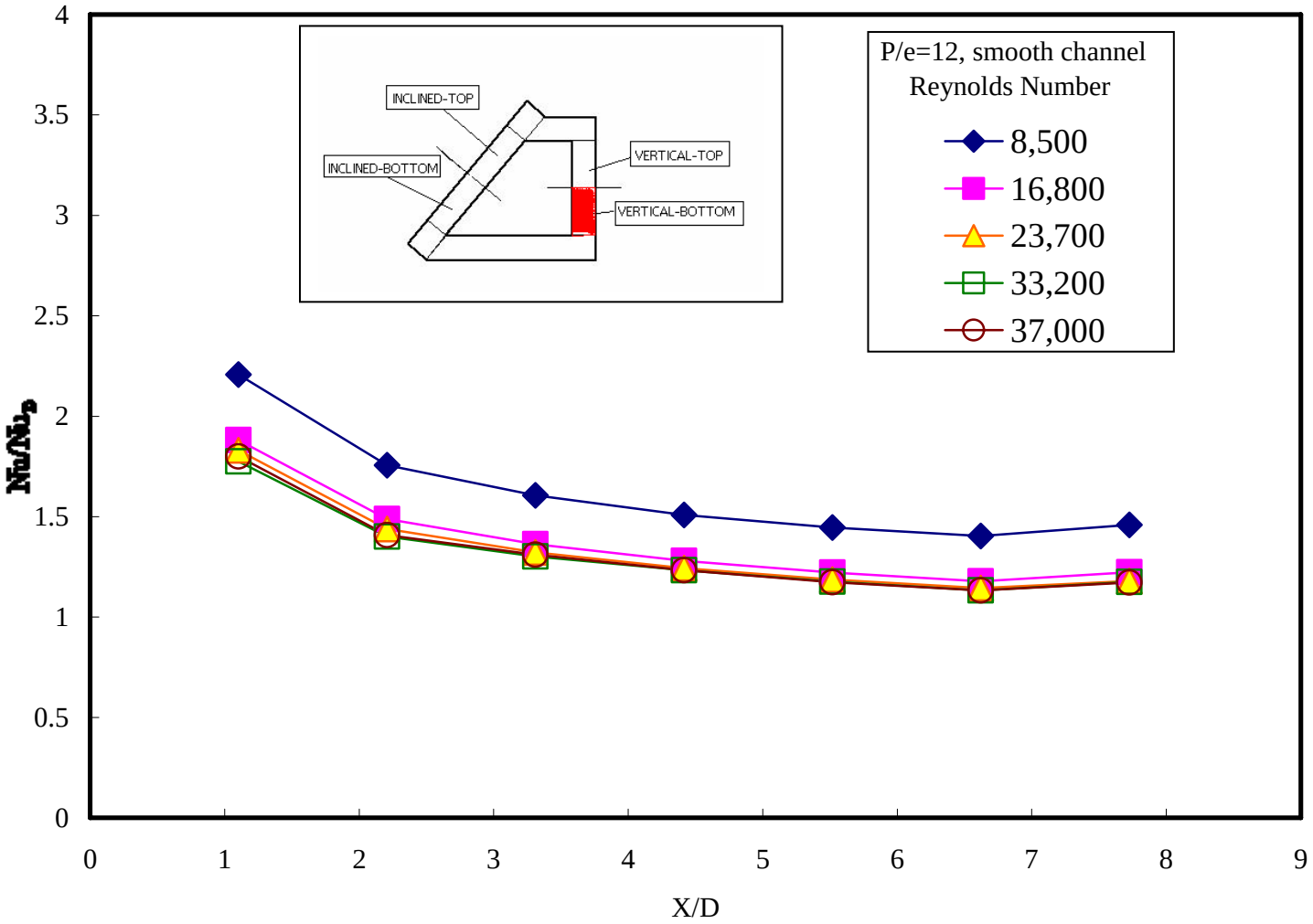

Fig. 11 Effect of Reynolds Number on Heat Transfer Distribution on Vert-Bot Wall in Smooth Channel

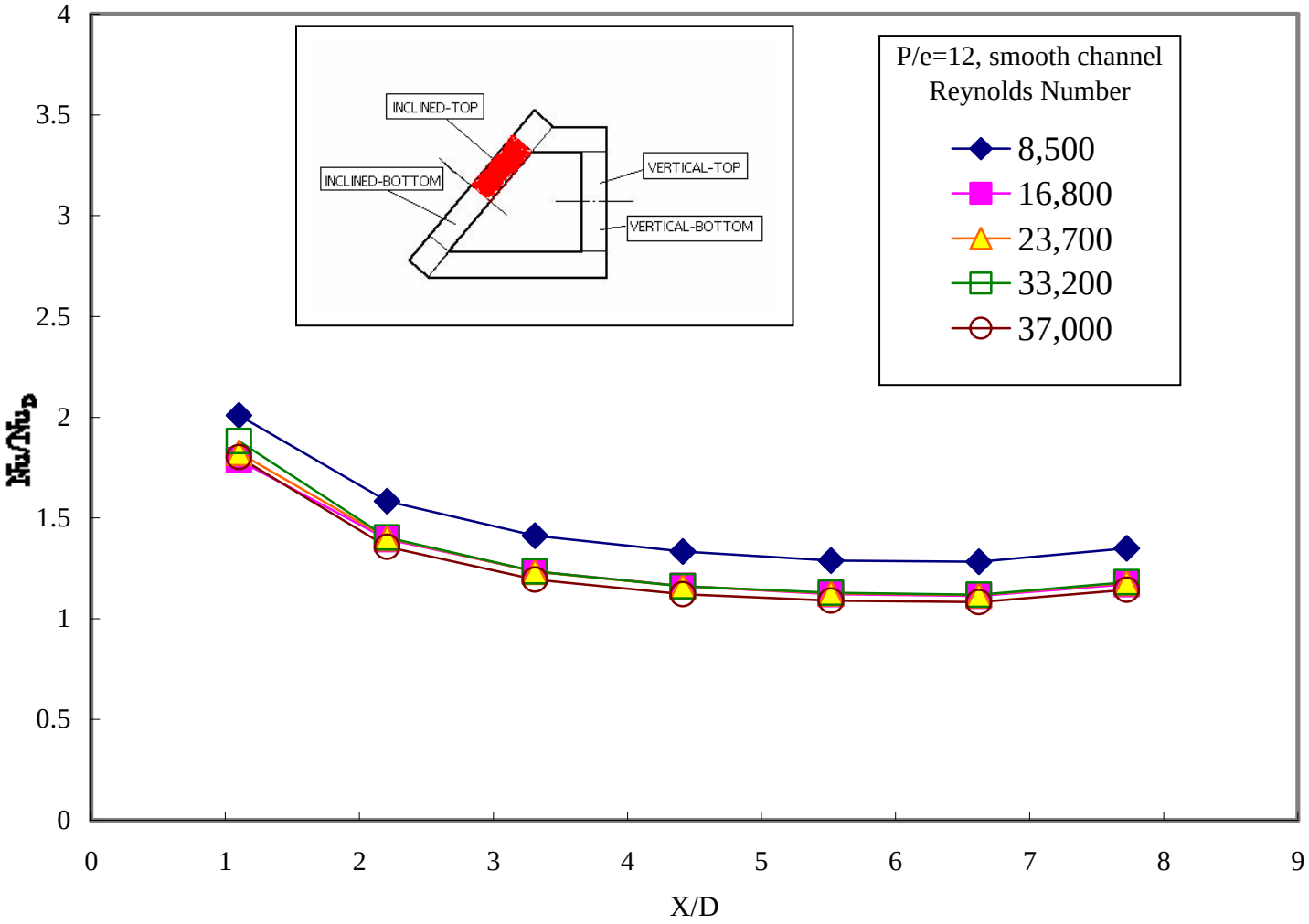

Fig. 12 Effect of Reynolds Number on Heat Transfer Distribution on Inc-Top Wall in Smooth Channel

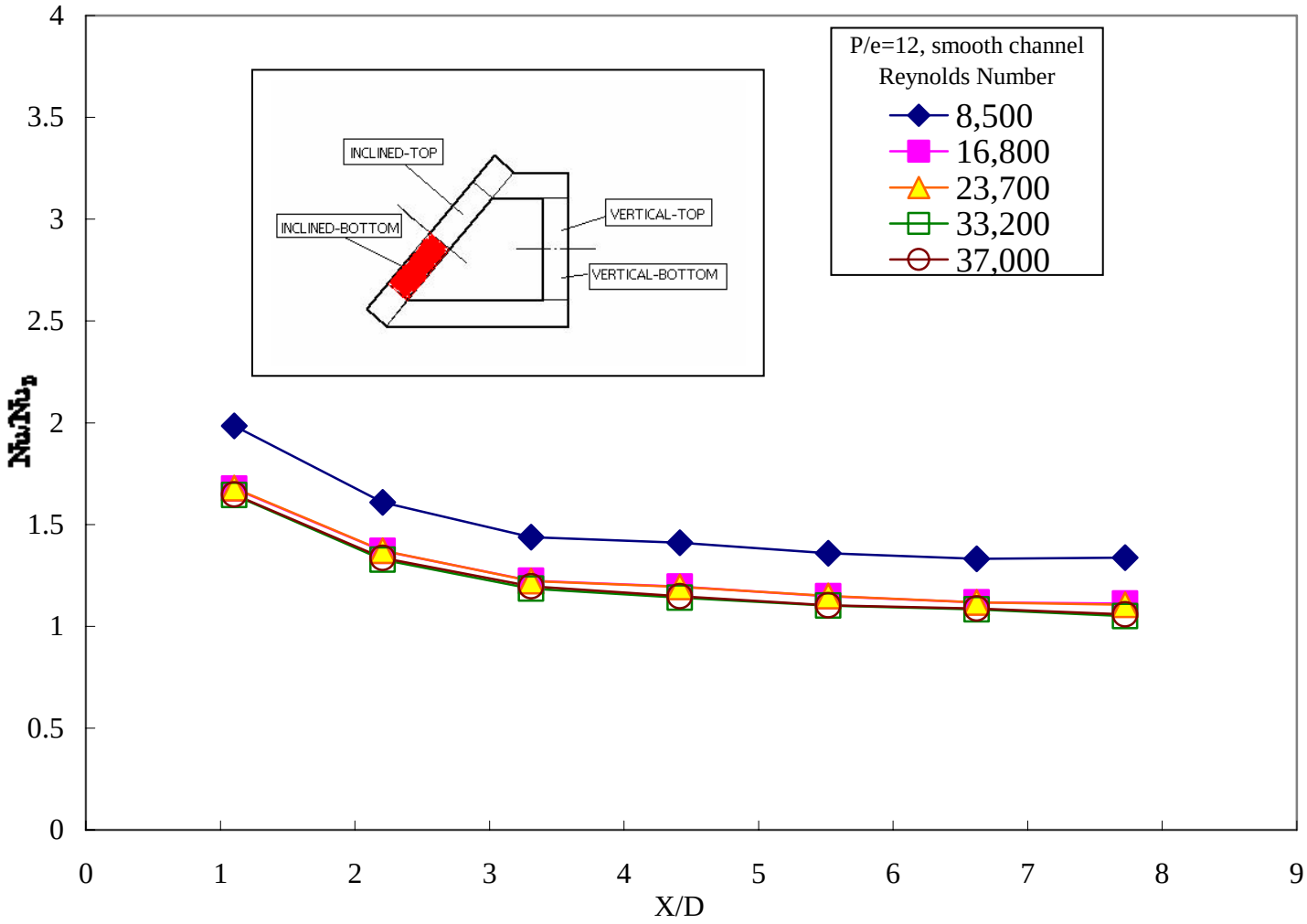

Fig. 13 Effect of Reynolds Number on Heat Transfer Distribution on Inc-Bot Wall in Smooth Channel

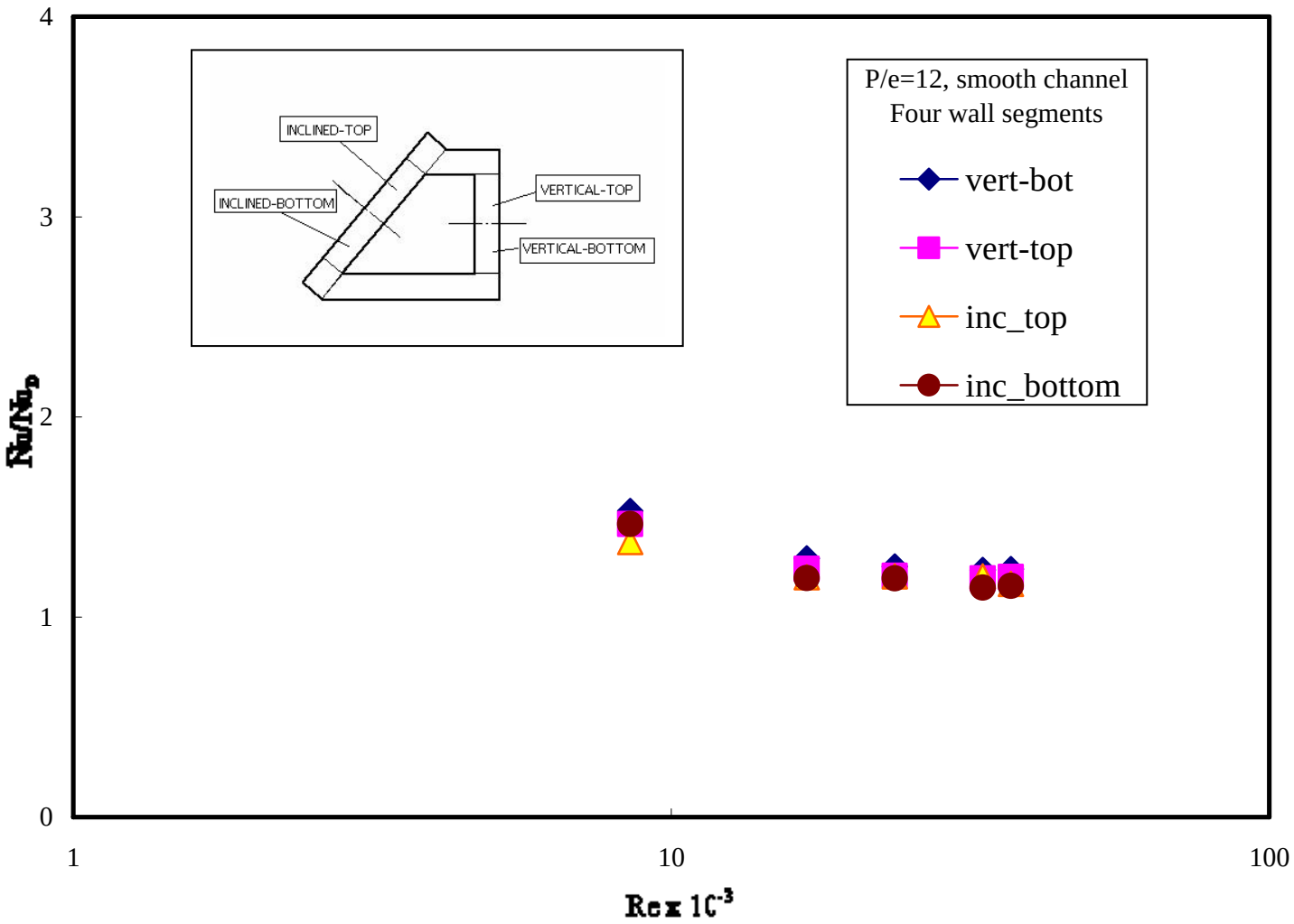

Fig. 14 Average Nusselt Number Ratio versus Reynolds Number on the Two Walls in Smooth Channel

The Nusselt number was found to vary from 38 to 100 and the Nusselt number ratio was found to vary from 1.1 to 2.25. The results were found to match with results obtained by Han [10] for the square channel.

In the case of smooth channel the variation of Nusselt number ratio with increasing Reynolds number is very small as there is no flow separation and reattachments in this case and so Reynolds number does not have any effect on the heat transfer augmentation. Therefore, the Nusselt number ratio for all five Reynolds number follow a similar trend on all the four walls. The Nusselt number ratio was found to approach unity along the streamwise direction in the fully developed region. The Nusselt number ratio was found to be highest for the lowest Reynolds number and lowest for the highest Reynolds number. It was found to vary between 2.25 and 1.1 along the axial direction. A variation of 5% in average Nusselt number was observed in the transverse direction on both the walls and the variation in average Nusselt number on all the four walls was found to be less than 10%.

Fig. 9 shows the graphical notation used to describe the walls in the test section. Each of the two aluminum walls consists of two rows of wall segments one at the top and the other at the bottom represented as VERT-TOP and VERT-BOT for one of the walls and INC-TOP and INC-BOT for the other wall inclined at 45°.

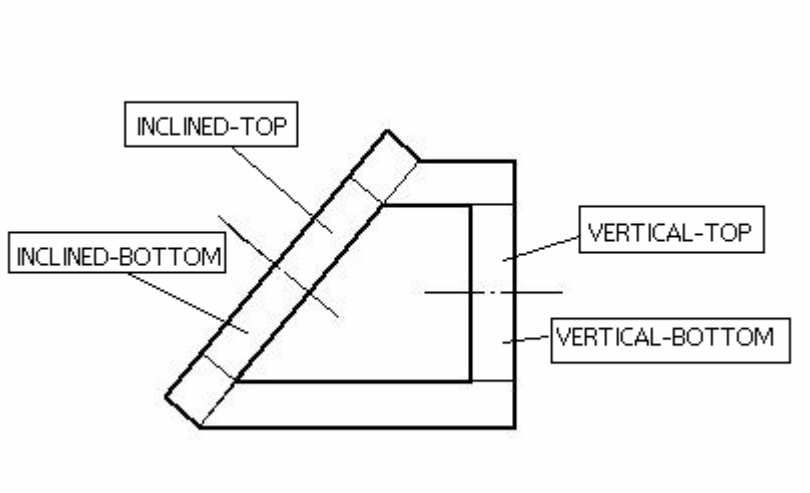

Fig. 9 Graphical Notation Used

Heat Transfer Distribution in Channel with 90° Transverse Ribs

The heat transfer and friction characteristic was studied for the same channel ribbed with 90° transverse ribs. The *P*/*e* ratio was maintained at 12 and was tested for five different Reynolds numbers. It was once again seen that Nusselt number ratio decreases with increase in axial distance and attains a constant value in the fully developed region as shown in Figs. 15-18.

The trend in Nusselt number ratio obtained was found to be similar to that of a smooth channel, except that there was 5%-15% fluctuation in the data obtained. The heat transfer augmentation at all Reynolds resulted in a 1.85-2.20 fold increase in comparison to the smooth channel.

The increase in heat transfer augmentation is due to the induced flow separation followed by reattachment by the ribs. The flow separation was thought to occur at the ribs and reattach downstream at about 6-8 times the rib height from the rib. It is also thought that a reverse flow boundary originates at the reattachment point and grows in thickness till the next flow separation occurred.

The Nusselt number variation in the transverse direction on the straight wall was less than 2% for the complete range of Reynolds number. In the case of inclined wall the variation in the Reynolds number was in the range of 7.5%-10%. On inclined wall the bottom wall had a lower heat transfer coefficient. This is probably due to the accumulation of hot fluid at the sharp corner of the trapezoid which prevents entry of cool fluid. This suppresses the effect created by flow separation at the ribs. Thus, giving rise to a larger variation in the Reynolds number on the inclined wall. This behavior was

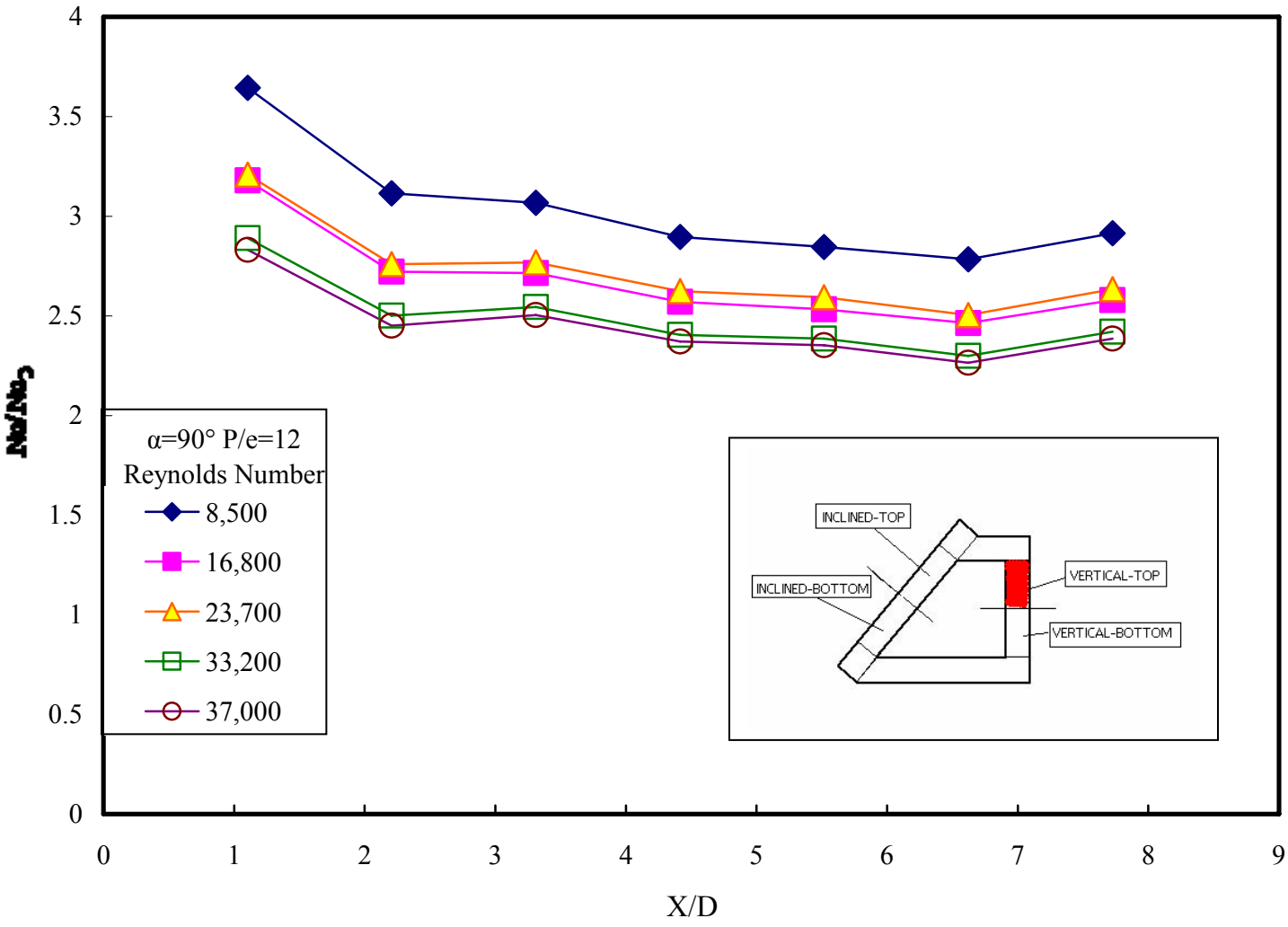

Fig. 15 Effect of Reynolds Number on Heat Transfer Distribution on Vert-Top Wall in Transverse Ribbed Channel

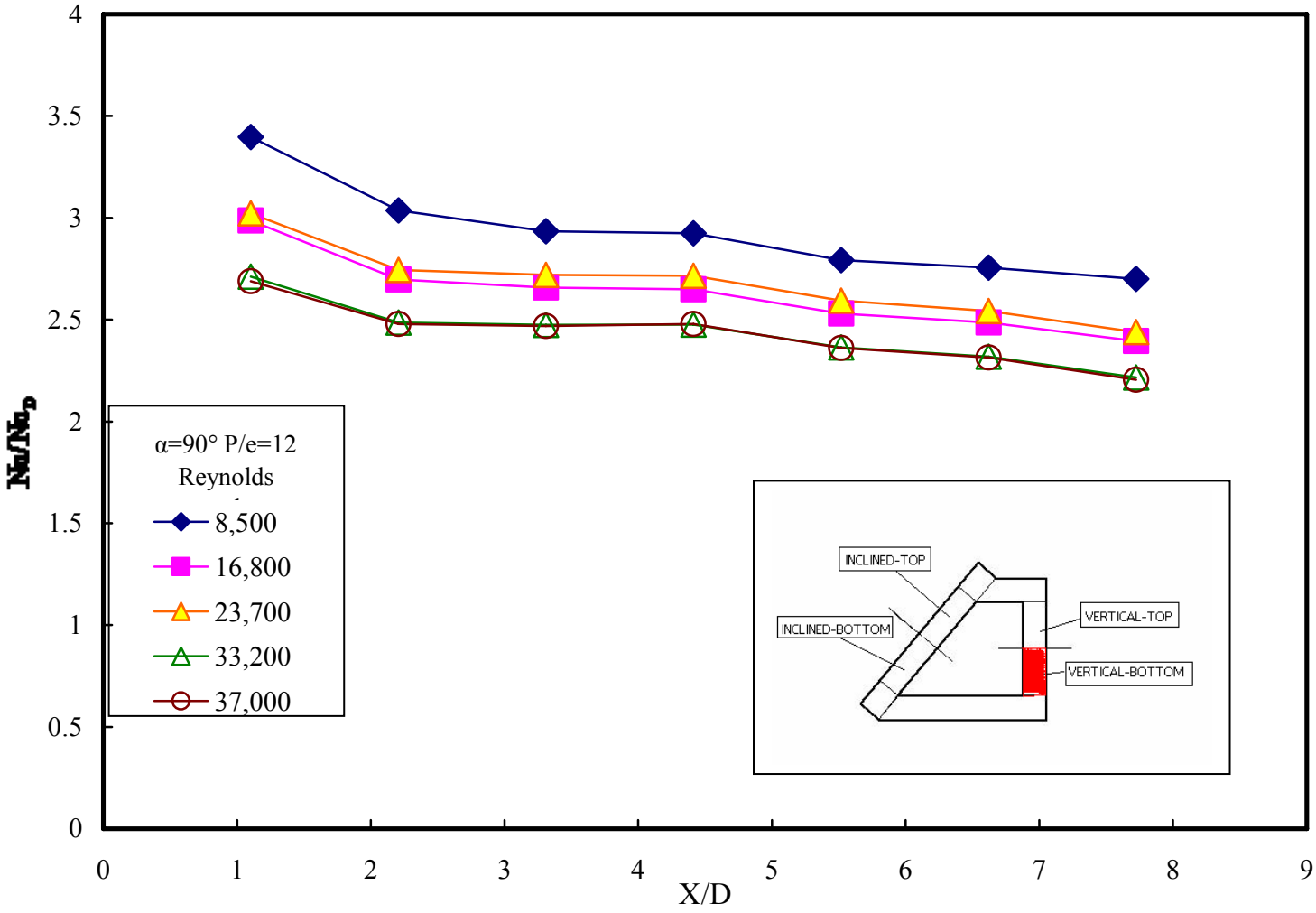

Fig. 16 Effect of Reynolds Number on Heat Transfer Distribution on Vert-Bot Wall in Transverse Ribbed Channel

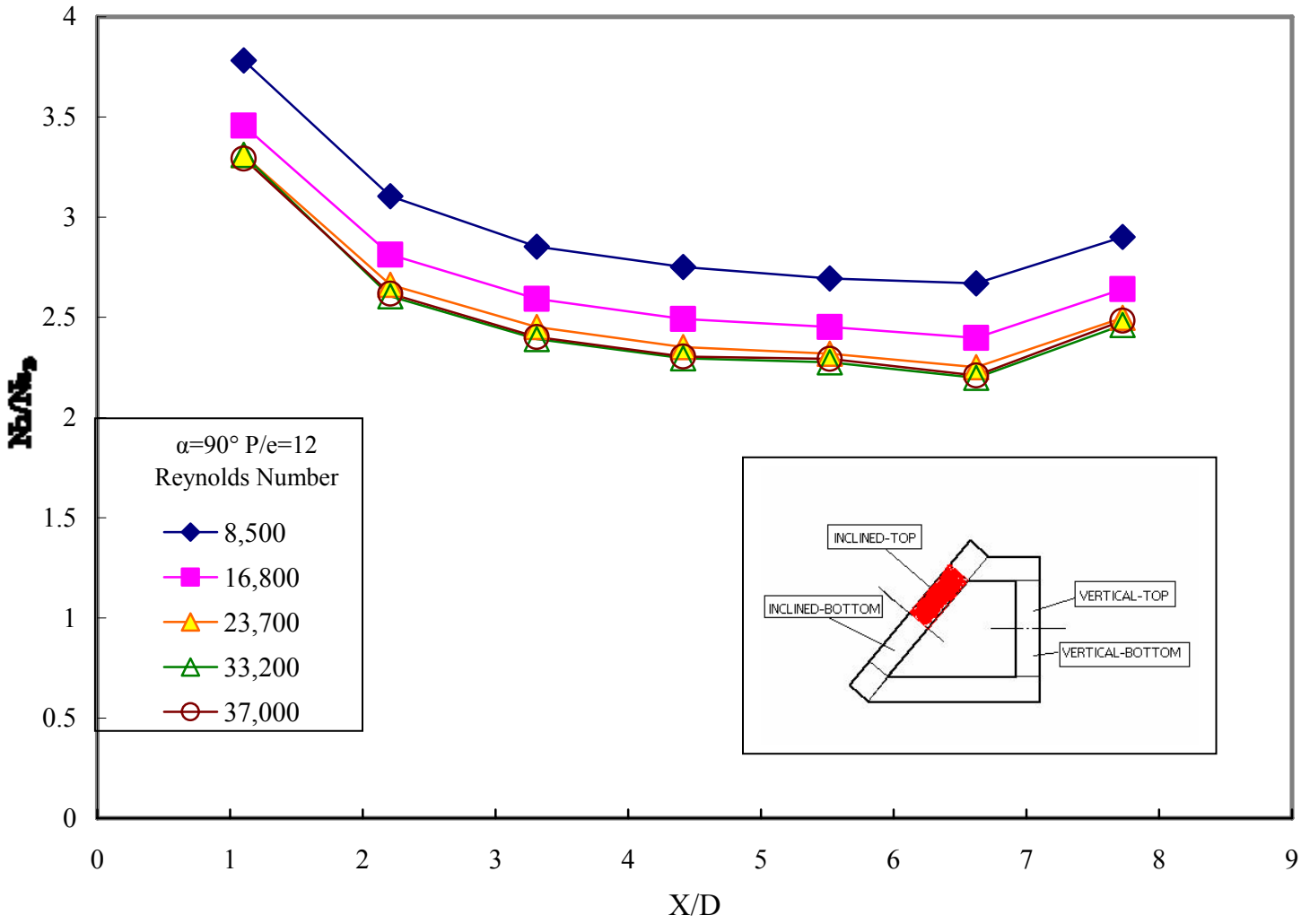

Fig. 17 Effect of Reynolds Number on Heat Transfer Distribution on Inc-Top Wall in Transverse Ribbed Channel

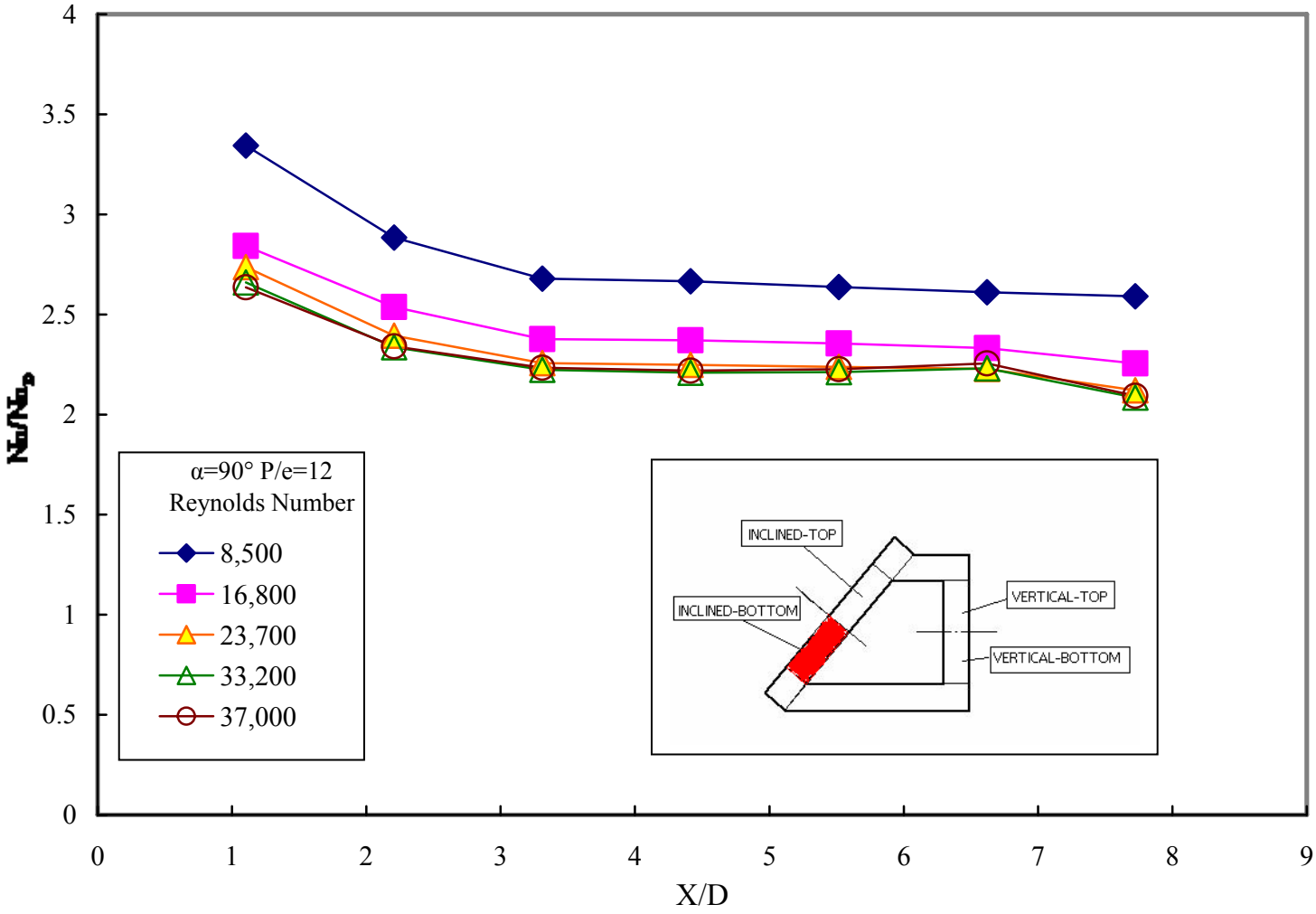

Fig. 18 Effect of Reynolds Number on Heat Transfer Distribution on Inc-Bot Wall in Transverse Ribbed Channel

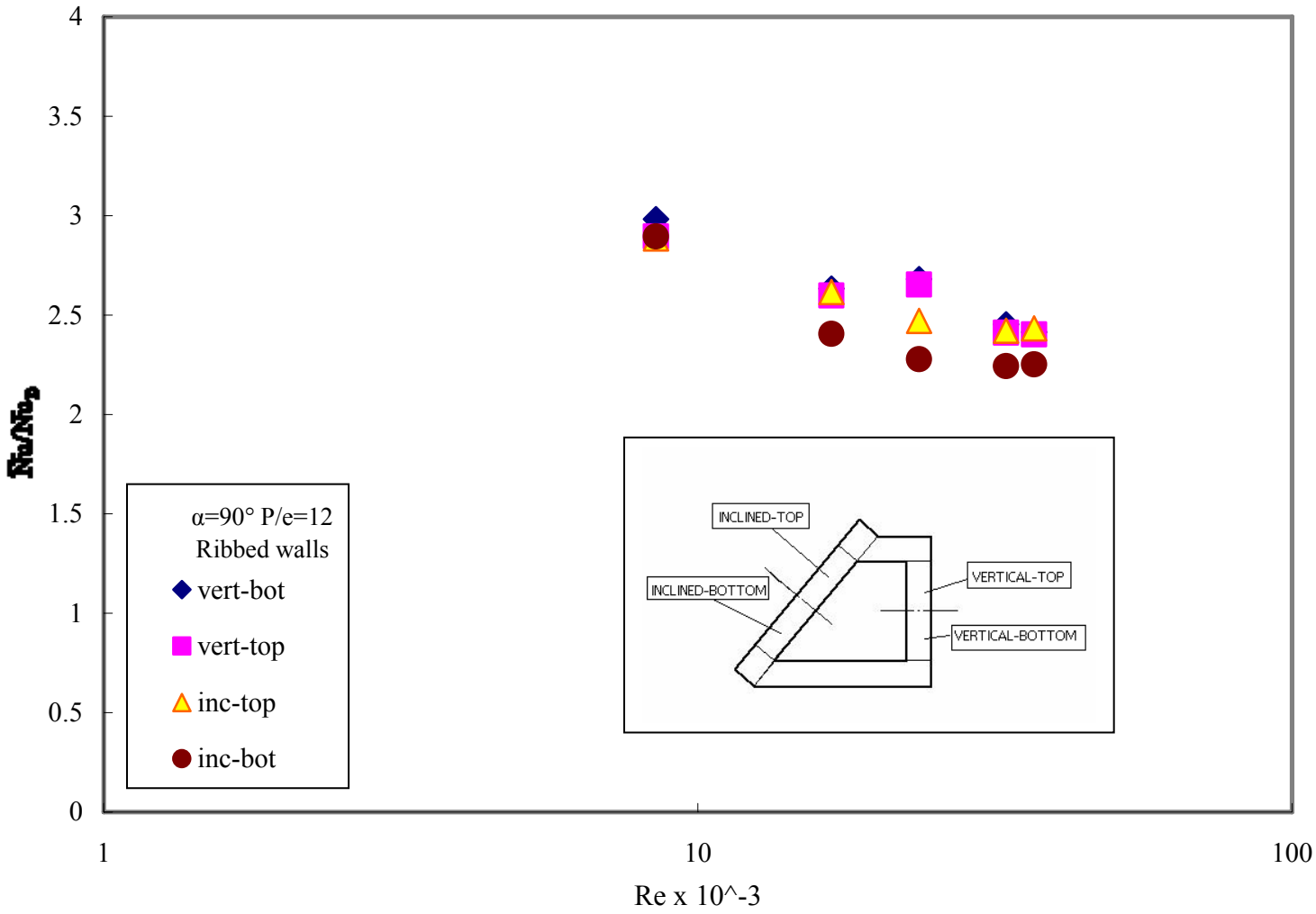

Fig. 19 Average Nusselt Number Ratio versus Reynolds Number on Two Walls in Transverse Ribbed Channel

also found in triangular channel by Metzer et al. [5]. It was also found that the geometry had a significant effect on the heat transfer coefficients on the four walls which resulted in 10-15 variation in the heat transfer among them because the bulk flow seemed to prefer the wider section as studied by Taslim [21].

The average Nusselt number on all four wall was wound to increase with increase in Reynolds number which is caused from better turbulence mixing. The increase in Reynolds number also causes an increase in the unsteady reverse flow just behind the rib which helps in better mixing. However, the Nusselt number ratio decreased appreciably with increase in Reynolds number as shown in Fig. 19. This is due to the fact that as Reynolds number increases the flow tends reattach quickly and so the effect on the heat transfer coefficient is considerably reduced. The study conducted by Liou et al. [12] showed that the increase in Nusselt number in a ribbed channel is proportional $Re^{0.6}$, whereas, in the case of fully developed turbulent flow in smooth circular tube correlated by McAdams/Dittus Boelter, the Nusselt number is proportional to $Re^{0.8}$. Therefore the rate of increase in Nusselt number in ribbed channel is less than that in smooth channel which results in the decrease of Nusselt number ratio with increase in Reynolds number.

The heat transfer augmentation in case of 90^{o} transverse ribs was found to be 100% more than that in a smooth channel for the complete range of Reynolds number. The uncertainty of Reynolds number was found to be close to 2% and that of the Nusselt number was found to be around 5%. The values were found to be within the uncertainty limit.

Heat Transfer Distribution in V-shaped Ribbed Channel

The heat transfer distribution on the trapezoidal channel with V-shaped ribs at 45° was studied and the characteristic curves were plotted as shown in Figs. 20-23. I was seen that the Nusselt number ratio along the stream wise direction behaved very similar to that in a square channel and channel ribbed with transverse ribs. The fluctuation in Nusselt number ratio was found to vary between 5%-20%. The heat transfer augmentation was found to increase by factor of 1.9 to 2.3 in comparison to the smooth channel and by a factor of 1.09 to 1.23 in comparison to the transverse ribbed channel. The increase in heat transfer coefficient is attributed to the induction of cross stream secondary flow which results in better turbulent mixing. The V-shaped ribs were also found to produce lesser pressure drop than the transverse ribs.

The Nusselt number ratio variation in the transverse direction on the straight walls was found to increase for 5% to 11% with increase in Reynolds number. However, the variation in the inclined wall was found be less than 6%. In both cases the heat transfer from the top wall was more than the bottom wall. The reason for this trend could be attributed to higher density of secondary flow near the top walls in comparison to that of the bottom wall which are separated by a greater distance than the top walls.

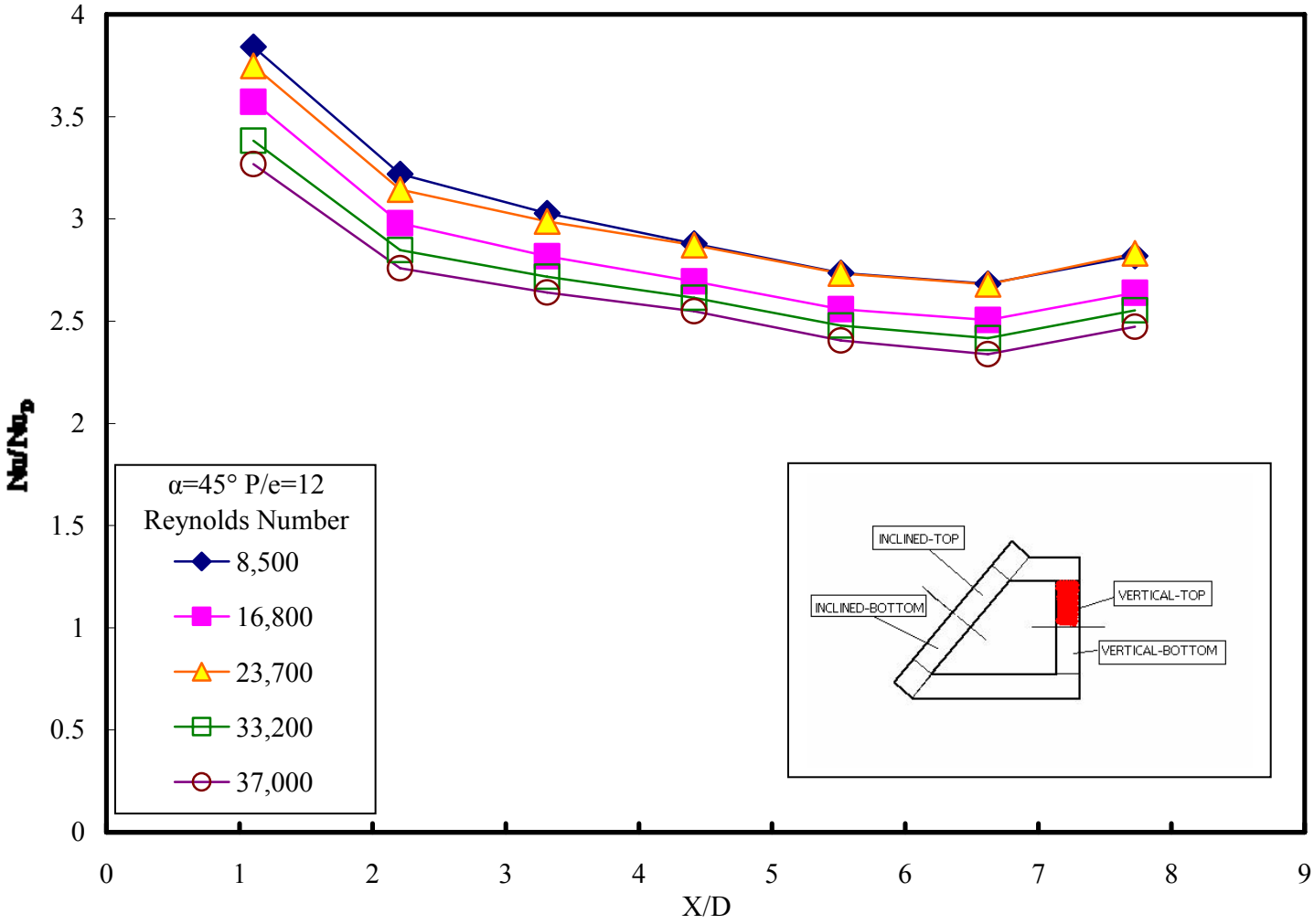

Fig. 20 Effect of Reynolds Number on Heat Transfer Distribution on Vert-Top Wall in V-shaped Ribbed Channel

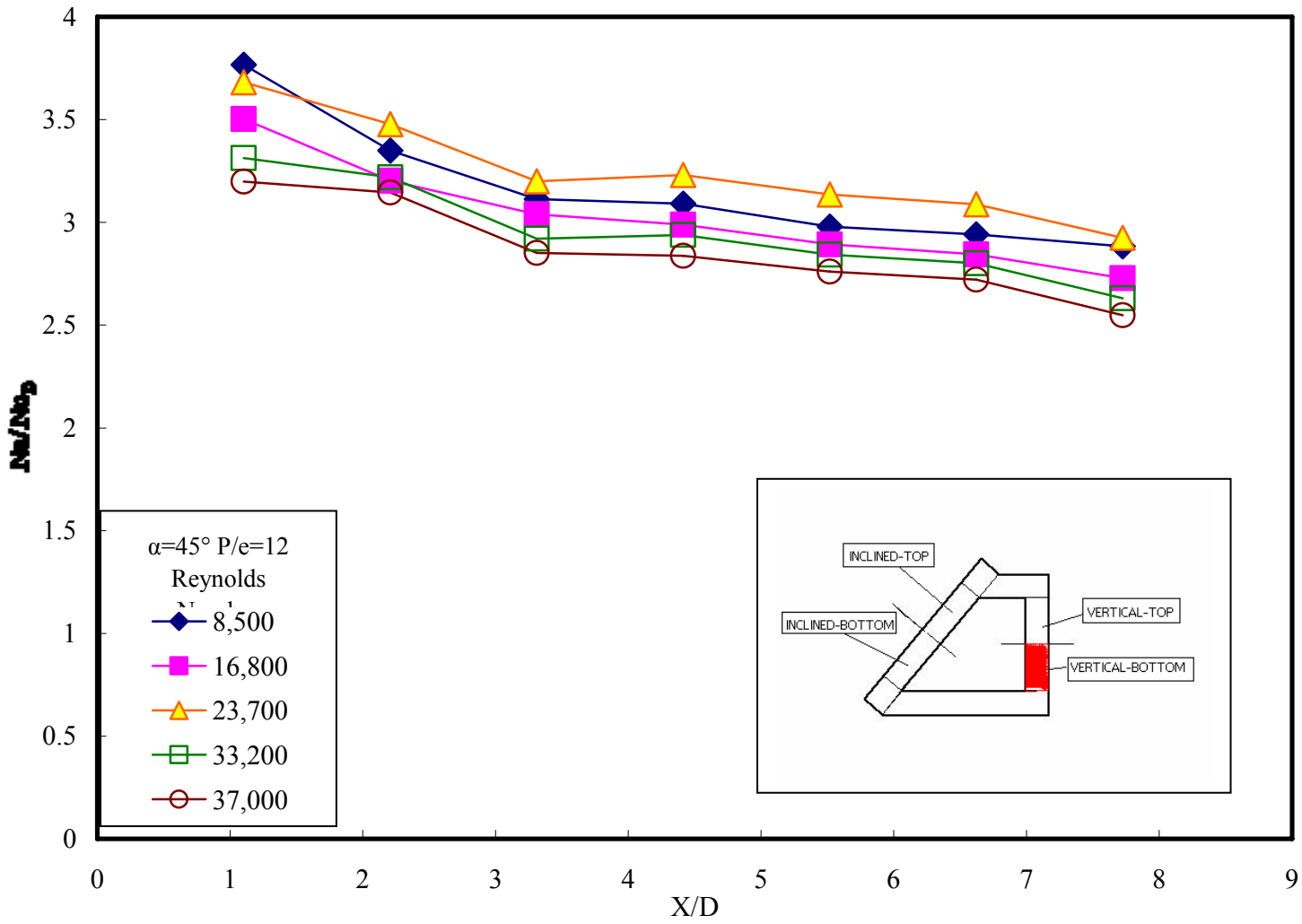

Fig. 21 Effect of Reynolds Number on Heat Transfer Distribution on Vert-Bot Wall in V-shaped Ribbed Channel

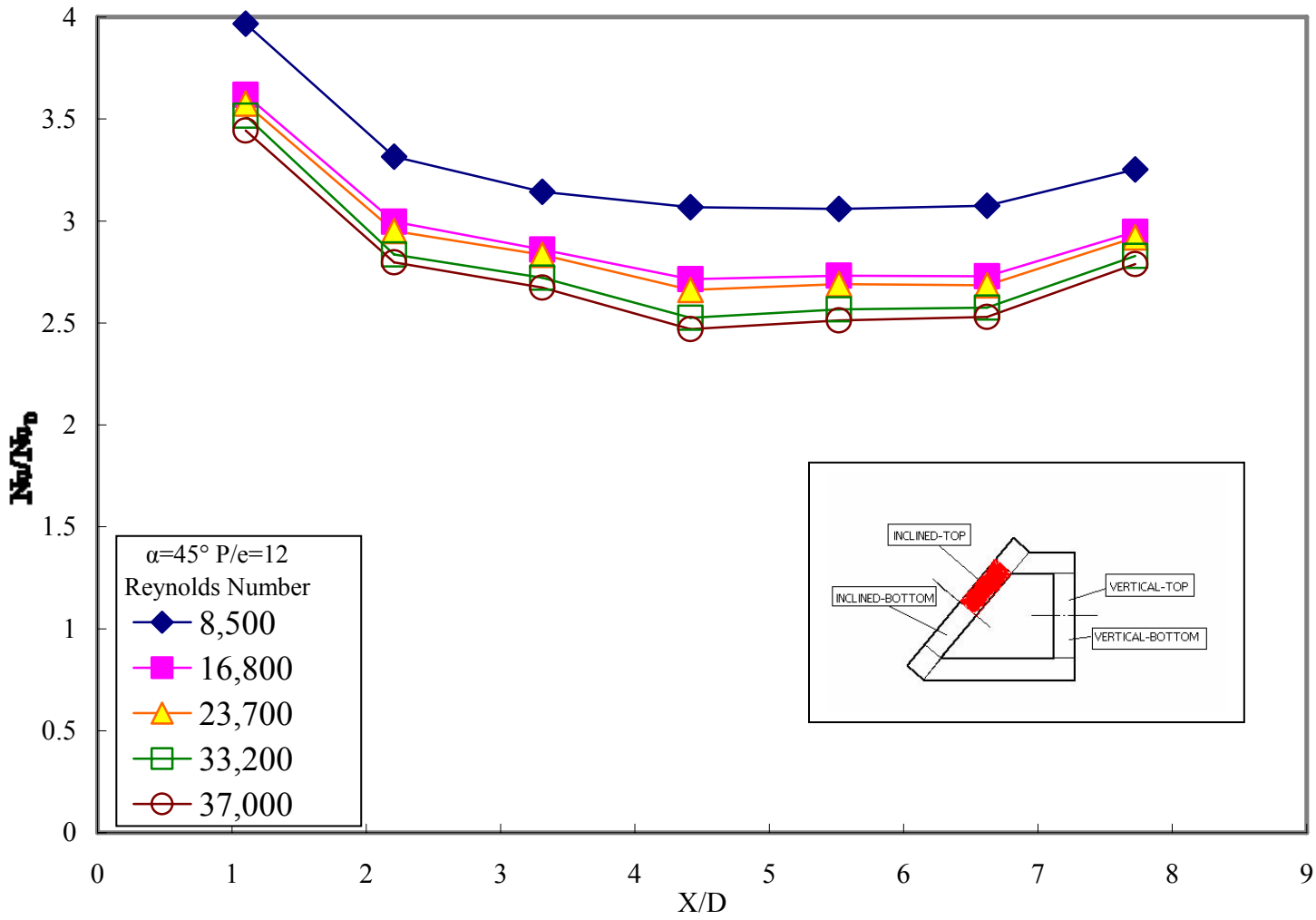

Fig. 22 Effect of Reynolds Number on Heat Transfer Distribution on Inc-Top Wall in V-shaped Ribbed Channel

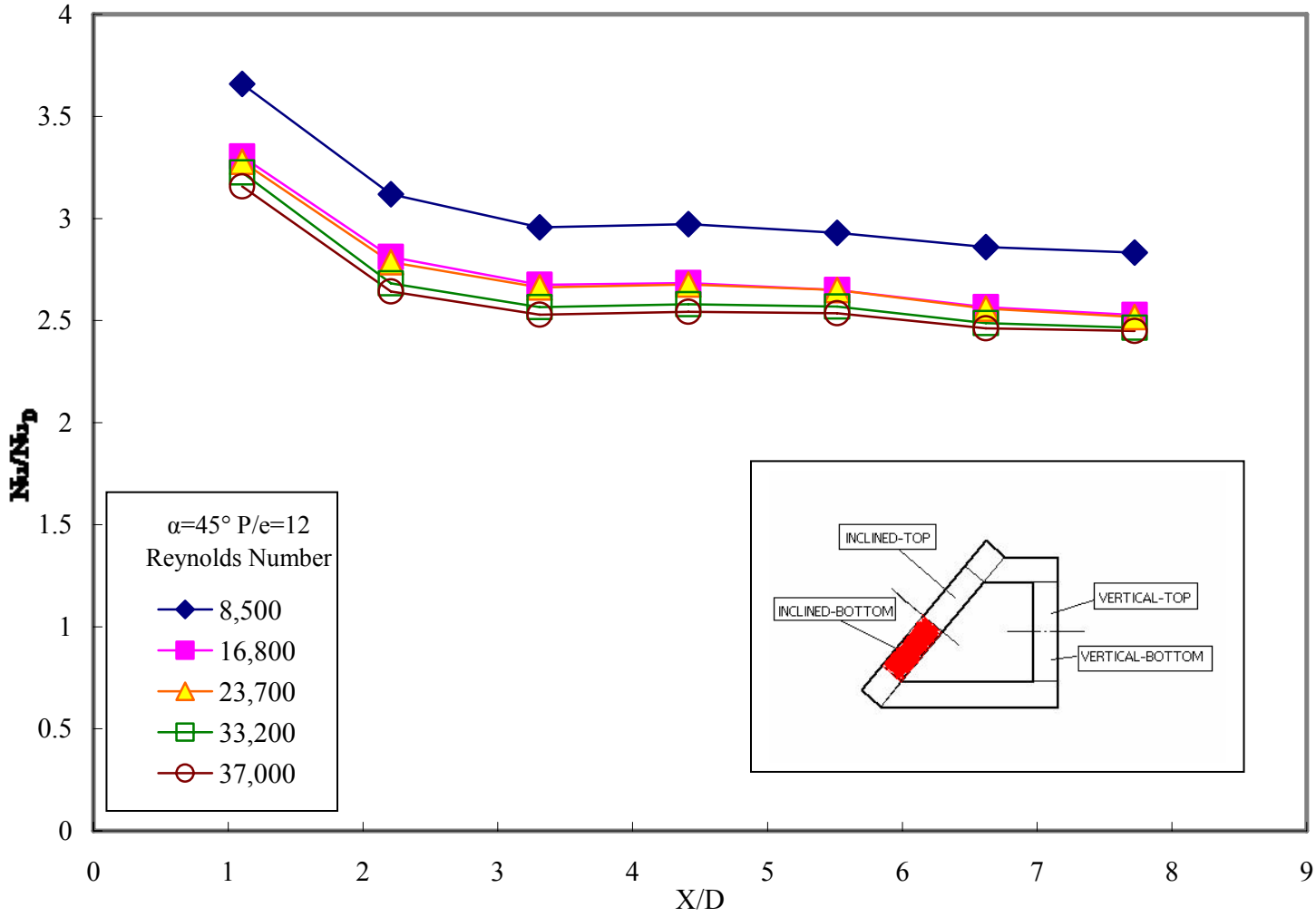

Fig. 23 Effect of Reynolds Number on Heat Transfer Distribution on Inc-Bot Wall in V-shaped Ribbed Channel

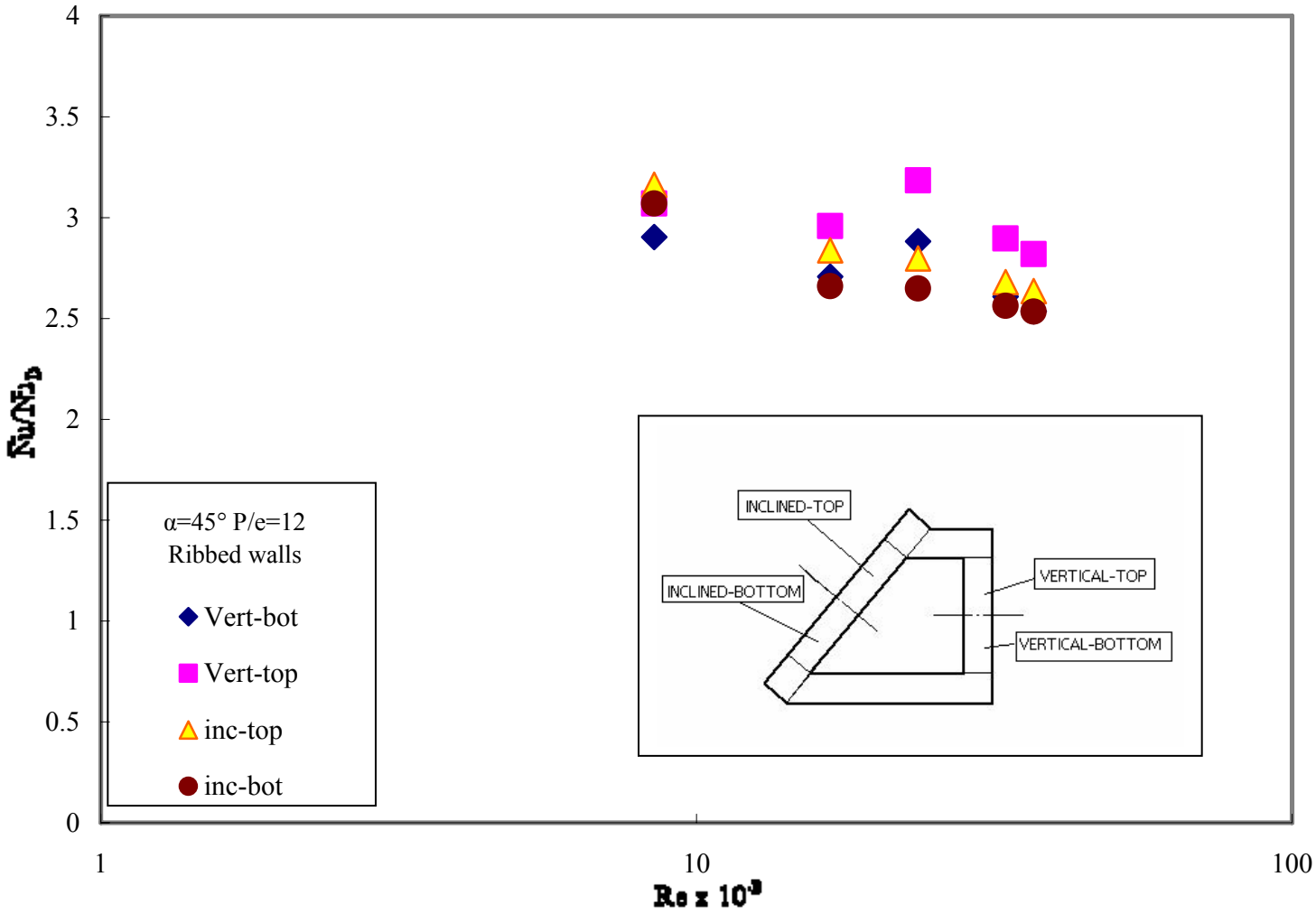

Fig. 24 Average Nusselt Number Ratio versus Reynolds Number on the Two Walls in V-shaped Ribbed Channel

The variation in Nusselt number in transverse direction in the inclined wall was found to be less than that in the straight wall is due to better turbulent mixing near the bottom wall on the inclined wall caused from the combination of cross stream secondary flow created by the V-shaped ribs and the flow separation at the ribs in comparison to the 90° transverse ribbed channel. However, the low Nusselt number on the bottom wall on the inclined side could be due to the reflection of secondary flows from the adjacent wall and accumulation of hot fluid in the sharp corner of the trapezoid which suppresses the effect of secondary flow caused from the ribs.

The average Nusselt number was once again found to decrease with increase in Reynolds number as shown in Fig. 24. As discussed in the earlier case, the rate of increase in Nusselt number with Reynolds number in ribbed channel is less than that in smooth channel because the mean flow energy is converted to turbulent kinetic energy which induces better mixing and in turn effective heat transfer. However, at low Reynolds number where the flow rate is low, there is no appreciable difference in the heat transfer augmentation in the four plates for both the ribbed configurations.

Friction Factor Characteristics for Various Rib Configurations

Figure 24 shows the variation of friction factor with Reynolds number for the smooth channel and the two ribbed channel investigated. The friction factor ratio was found to increase with increase in Reynolds number due to the resistance offered to the flow of fluid as given in Table 1. The heat transverse augmentation was found to vary between 2-2.5 for the transverse rib and 2.5-3 for the V-shaped rib. This enhancement in both the cases was accompanied by pressure drop penalty of 2.5 to 4 on the V-shaped ribbed channel and 4 to 5 on the 90° transverse ribbed channel. The 90° transverse ribs produced 25 % to 60% higher pressure drop when compared to the V-shaped ribs at 45° for the complete range of Reynolds number investigated. The results obtained were in accordance with previously obtained data by Chandra [19].

Table 1 Friction Factor Ratio for Cases Investigated

Reynolds Number	Transverse Ribs	V-shaped Ribs
8,500	4.018	2.410
16,800	4.100	3.106
23,700	4.189	3.434
33,200	4.479	3.416
37,000	4.796	3.573

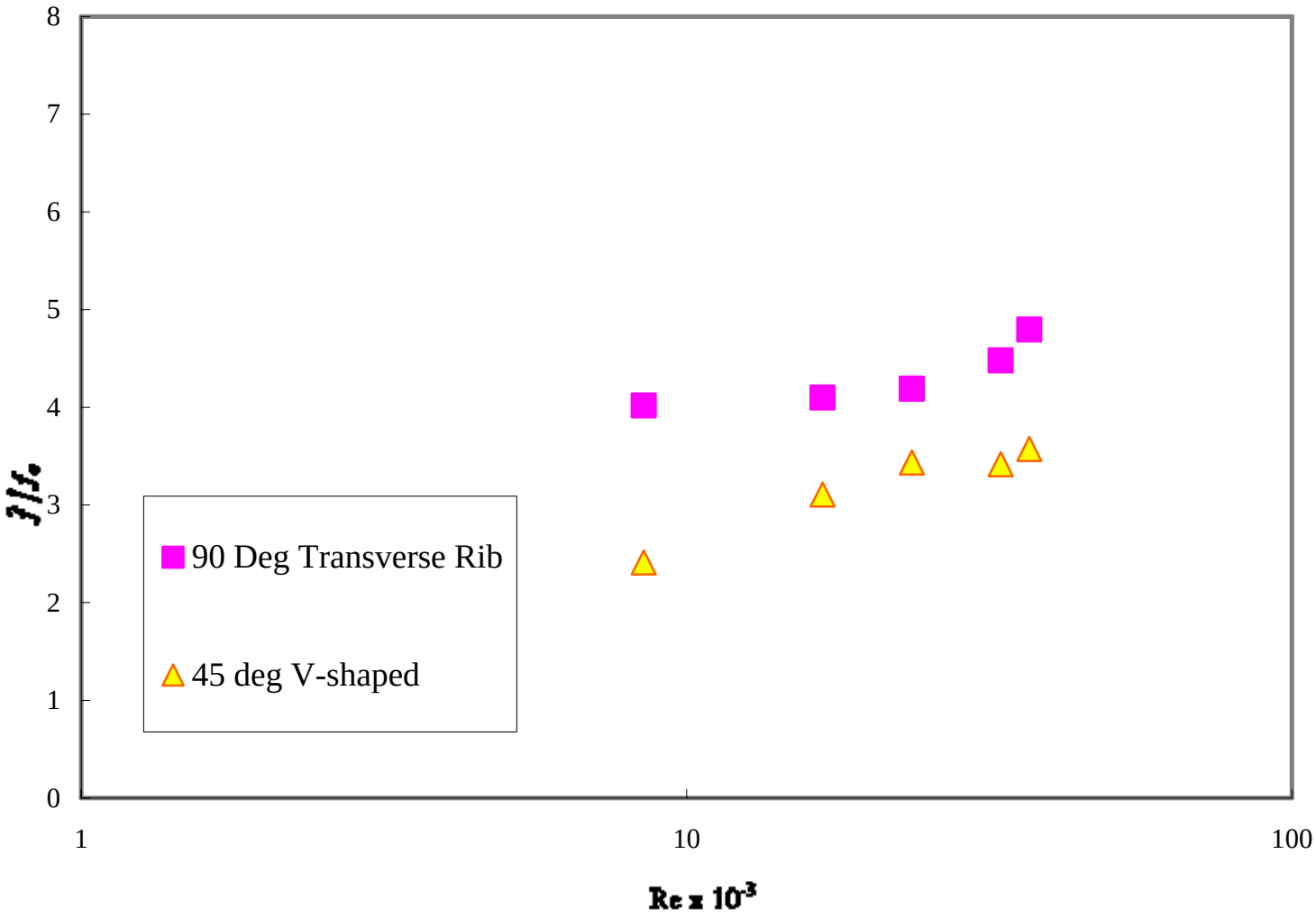

Fig. 25 Average Friction Factor Ratio versus Reynolds Number for Various Rib Configurations

Heat Transfer Performance

The thermal performance comparison for different rib configuration on the four walls was plotted as shown in Figs. 25-28. The Nusselt number ratio was plotted against the friction factor ratio for the entire range of Reynolds number. As discussed in the earlier section the Nusselt number ratio decreased with increase in Reynolds Number, whereas the friction factor ratio increased with increase in the Reynolds number. Form this it is deduced that the performance decreases with increase in Reynolds number.

The thermal performance is also represented in Table 2-3 on different wall segments using thermal performance correlation for various Reynolds number. It was once again seen that the performance decreased with increase in Reynolds number. It was also noted that on all the four wall segments the thermal performance for the smooth channel was increasing with increasing Reynolds number in comparison to the ribbed channel. This is due to the higher rate of increase in friction penalty, in turn, the pump power with increase in the Reynolds number in comparison to the heat transfer augmentation.

The heat transfer enhancement for the 90° transverse ribs was found to be carrying at 2.25 to 2.75 on the four walls and the pressure drop penalty was found to vary between 4 and 5. In the case of the V-shaped ribs the heat transfer enhancement was found to be ranging from 3.25 to 25 and the friction factor ratio was between 2 and 4.

It is found that there is only small lateral variation in the heat transfer on the straight wall whereas the variation on the inclined wall was found to be around 15% in

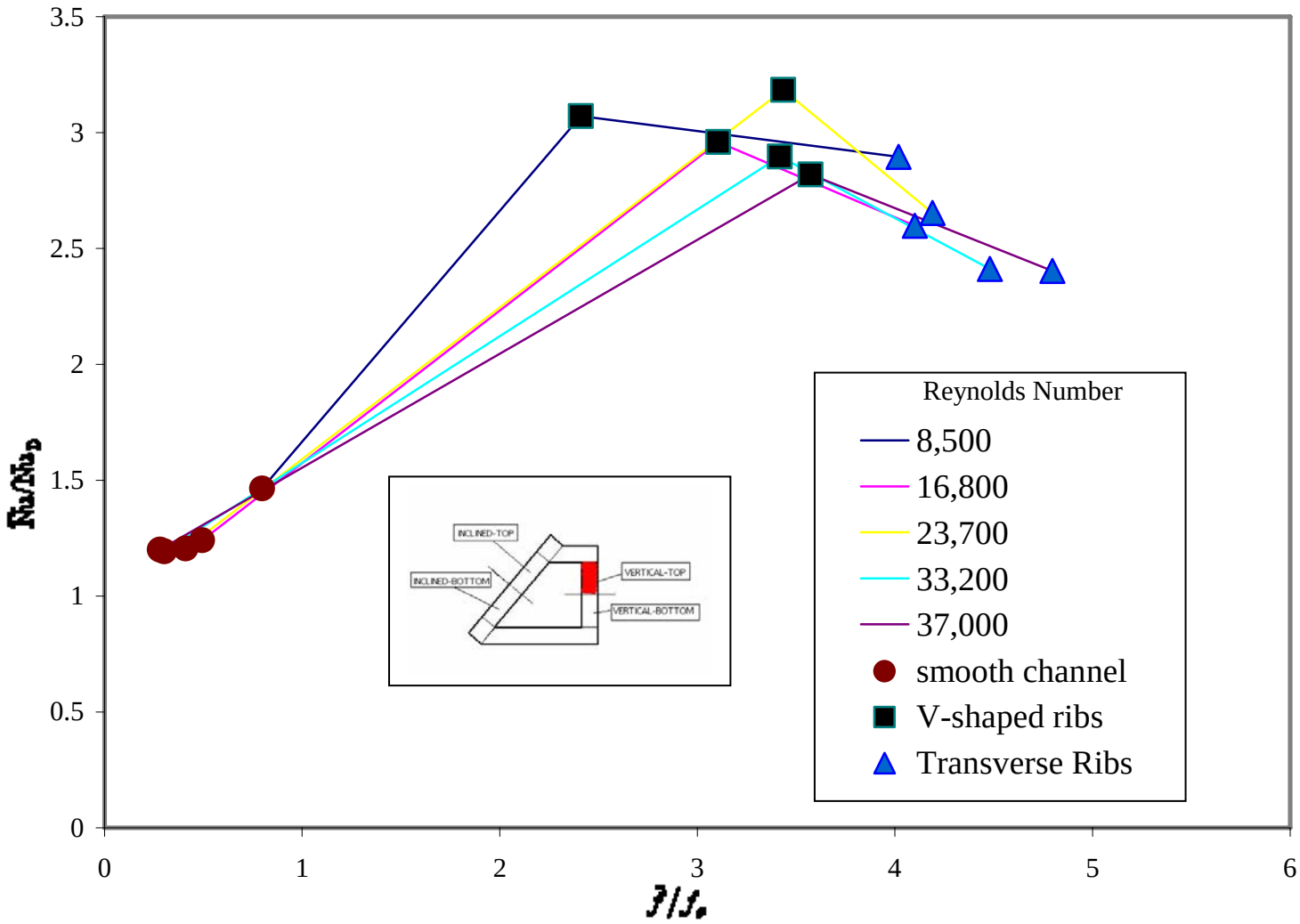

Fig. 26 Average Nusselt Number Ratio versus Friction Factor Ratio for Vert-Top Wall

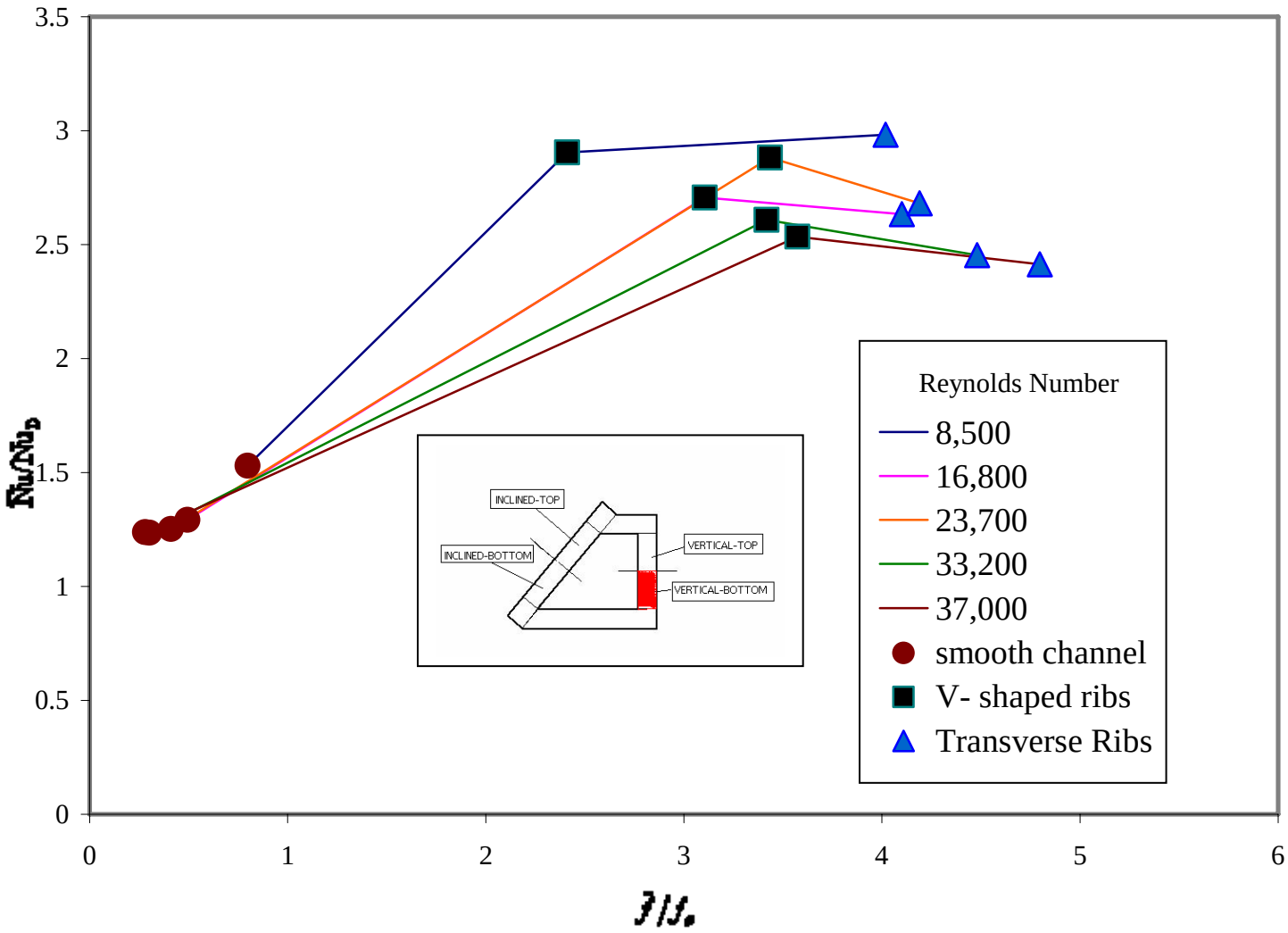

Fig. 27 Average Nusselt Number Ratio versus Friction Factor Ratio for Vert-Bot Wall

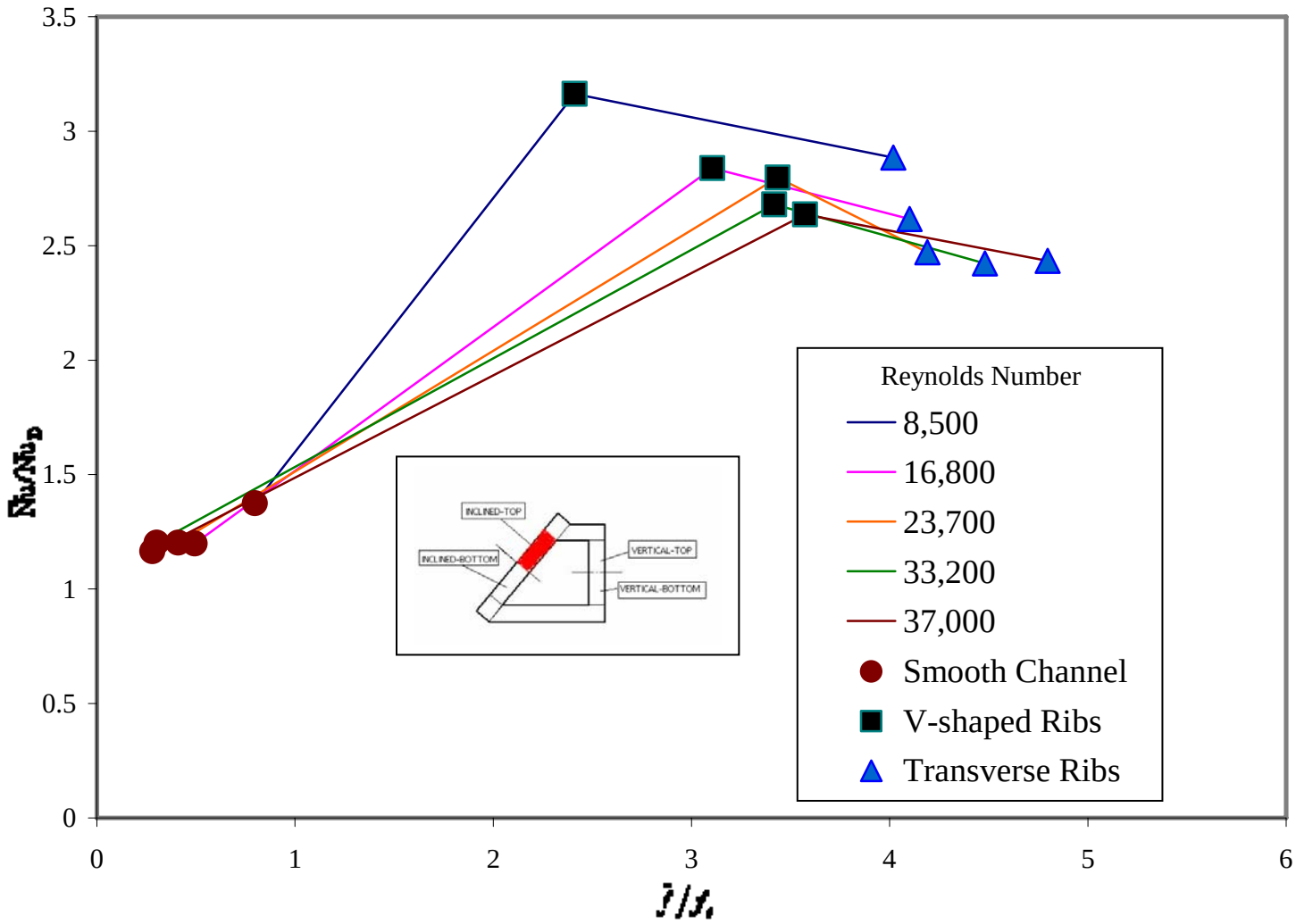

Fig. 28 Average Nusselt Number Ratio versus Friction Factor Ratio for Inc-Top Wall

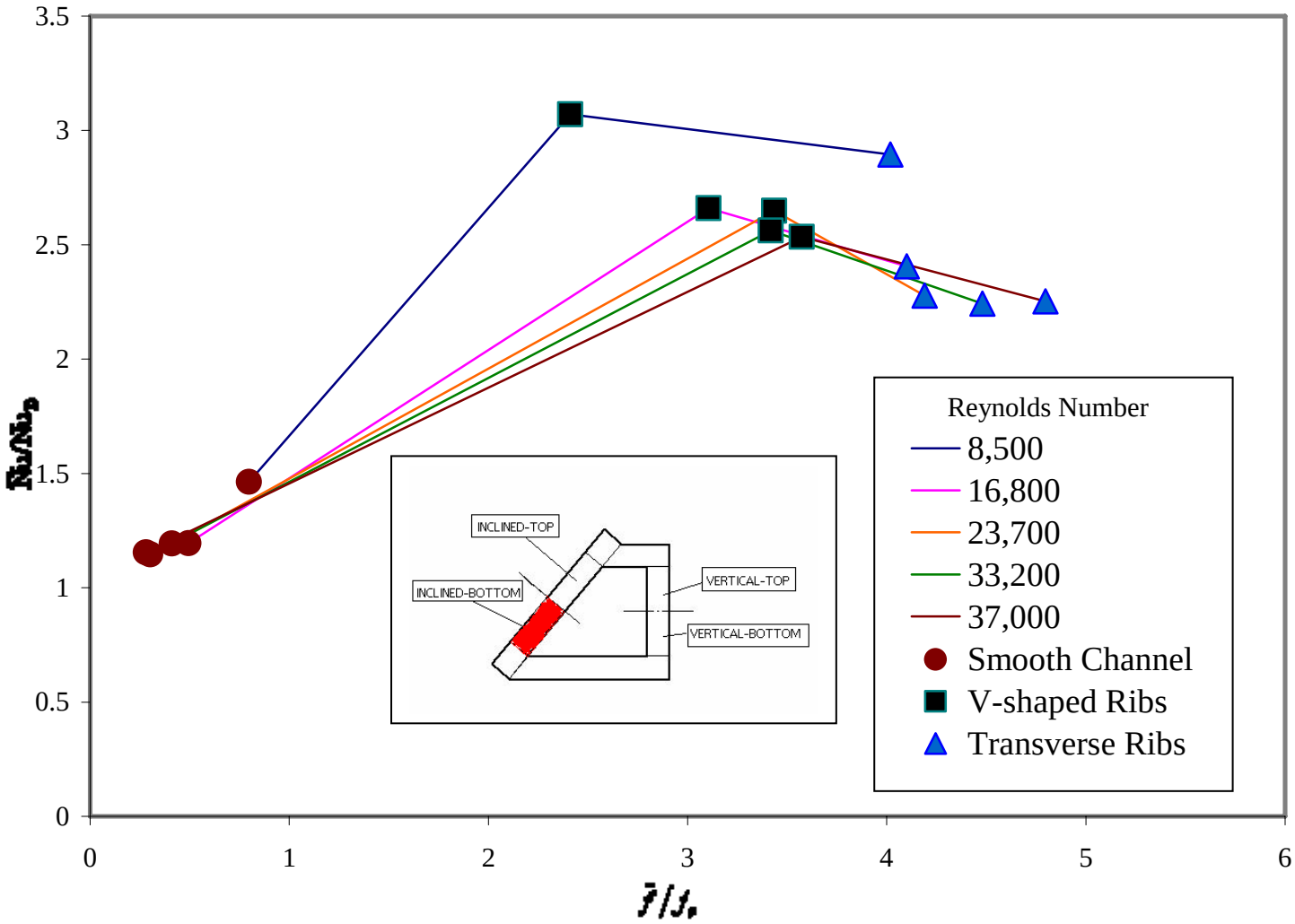

Fig. 29 Average Nusselt Number Ratio versus Friction Factor Ratio for Inc-Bot Wall

Table 2 Thermal Performance on the Vertical Wall Segment

	Vertical-Top Wall Segment		Vertical-Bottom Wall Segment	
Re	Transverse Ribs	V-shaped Ribs	Transverse Ribs	V-shaped Ribs
	90 Deg	45 Deg	90 Deg	45 Deg
8,500	1.82	2.29	1.88	2.17
16,800	1.62	2.03	1.65	1.86
23,700	1.65	2.11	1.66	1.91
33,200	1.46	1.92	1.49	1.73
37,000	1.43	1.84	1.43	1.66

Table 3 Thermal Performance on the Inclined Wall Segment

	Inclined-Top wall Segment		Inclined-Bottom wall segment	
Re	Transverse Ribs	V-shaped Ribs	Transverse Ribs	V-shaped Ribs
	90 Deg	45 Deg	90 Deg	45 Deg
8,500	1.81	2.36	1.82	2.29
16,800	1.63	1.95	1.5	1.82
23,700	1.53	1.85	1.41	1.76
33,200	1.47	1.78	1.36	1.7
37,000	1.44	1.72	1.34	1.66

case of transverse ribs. In case of the V-shaped ribs the variation is significant on both the straight and the inclined wall and was close to 10%. So, from the graph it is clear that the V-shaped ribs produced 20% higher heat transfer enhancement but also resulted in 25%-60% lesser pressure drop penalty.

It was observed that at high Reynolds number the bottom wall segments on the inclined wall always resulted in poor performance due to the accumulation of slowed-heated fluid also referred as vortices near the sharp corner of the trapezoid.

SUMMARY AND CONCLUSIONS

The average heat transfer and friction characteristics measurement was performed in a trapezoidal channel; with 90° transverse ribs and V-shaped ribs angled at 45° for Reynolds number ranging from 7,000 to 40,000 with a P/e ratio of 12 and e/D_h ratio of 0.016. The main findings are as follows

1) For the smooth channel, channel ribbed with 90° transverse ribs and 45° V-shaped ribs, the Nusselt number ratio decreased with increase in axial distance and reached a constant value a few ribs downstream of the channel from the entrance.
2) The 45° V-shaped produced 20% better heat transfer augmentation than the 90° transverse ribs and 120% better heat transfer augmentation than the smooth channel for the complete range of Reynolds number due to the induction of the cross stream secondary flow which augments the heat removal.
3) The V-shaped ribs produced 25%-60% less pressure drop than the 90° transverse ribs for the complete range of Reynolds number.
4) The thermal performance on all the four wall segments was found to decrease with increase in Reynolds number due to higher friction losses.
5) The heat transfer on ribbed walls at sharp corners was found to be low due to the slowed and heated boundary layer formation at the corners which results in accumulation of hot fluid.

REFERENCES

1. Dippery, D. F., Sabersky, R. H., “Heat and Momentum Transfer in Smooth and Rough Tubes in Various Prandtl Number,” *International Journal of Heat and Mass Transfer*, Vol. 6, 1963, pp. 329-353.

2. Han,J. C., Glicksman, L. R., Rohsenow, W. M., “An Investigation of Heat Transfer and Friction for Rib Roughened Surfaces,” *International Journal of Heat and Mass Transfer*, Vol. 21, 1978, pp. 1143-1156.

3. Han, J. C., “Heat Transfer and Friction in Channel with Two Opposite Rib-Roughened Walls,” *Journal of Heat Transfer*, Vol. 106, No. 4, 1984, pp. 774-781.

4. Han, J. C., Park, J. S., Lei, C. K., “Heat Transfer Enhancement in Channel with Turbulent Promoters,” *Journal of Engineering for Gas Turbines and Power*, Vol. 107, 1985, pp. 628-635.

5. Metzger, D. E., Vedula, R. P., “Heat Transfer in Triangular Channel with Angled Roughness Ribs on Two Walls,” *Experimental Heat Transfer*, Vol. 1, 1987, pp. 31-44.

6. Luo, D. D., Leung, C. W., Chan, T. L., “Forced Convection and Flow Friction Characteristics of Air Cooled Horizontal Equilateral Triangular Ducts with Ribbed Internal Surfaces,” *International Journal of Heat and Mass Transfer*, Vol. 47, 2004, pp. 5439-5450.

7. Han, J. C., Park J. S., “Developing Heat Transfer in Rectangular Channels with Rib Turbulators,” *International Journal of Heat and Mass Transfer*, Vol. 31, No. 1, 1988, pp. 183-195.

8. Han, J. C., “Heat Transfer and Friction Characteristics in Rectangular Channel with Rib Turbulators,” *Journal of Heat Transfer*, Vol. 110, 1988, pp. 321-328.

9. Lau, S. C., McMillian, R. D., Han, J. C., “Turbulent Heat Transfer and Friction in a Square Channel with Discrete Rib Turbulators,” *Heat Transfer in Gas Turbine Engines*, 1989, pp. 33-41.

10. Han, J. C., Zhang, Y. M., Lee, C. P., “Augmented Heat Transfer in Square Channel with Parallel, Crossed and V-Shaped Angled Ribs,” *Journal of Heat Transfer*, Vol. 113, 1991, pp. 590-596.

11. Lau, S. C., Kukreja, R. T., McMillian, R. D., “Effect of V-Shaped Rib Array on Turbulent Heat Transfer and Friction of Fully Developed Flow in a Square Channel,” *International Journal Heat Mass Transfer*, Vol. 34, No. 7, 1991, pp. 1605-1616.

12. Liou, T. M., Hwang, J. J., “Turbulent Heat Transfer Augmentation and Friction in Periodic Fully Developed Channel Flow,” *ASME Journal of Heat Transfer*, Vol. 114, 1992, pp. 56-64.

13. Han, J. C., Zhang, Y. M., Lee C. P., “Influence of Surface Heat Flux Ratio on Heat Transfer Augmentation in Square Channel with Parallel, Crossed and V-Shaped Angled Ribs,” *ASME Journal of Turbomachinery*, Vol. 114, 1992, pp. 872-880.

14. Taslim, M. E., Spring, S. D., “Effects of Turbulator Profile and Spacing on Heat Transfer and Friction in a Channel,” *Journal of Thermophysics and Heat Transfer*, Vol. 8, 1994, pp. 555-562.

15. Taslim, M. E., Li, T., Kercher, T. M., “Experimental Heat Transfer and Friction in Channel Roughened with Angled, V-Shaped and Discrete Ribs on Two Opposite Walls,” *ASME Journal of Turbomachinery*, Vol. 118, 1996, pp. 20-28.

16. Katoh, K., Kwing S. C., Azuma, T., “Heat-Transfer and Pressure Loss by Surface Roughness in Turbulent Channel Flows,” *International Journal of Heat and Mass Transfer*, Vol. 43, 2000, pp. 4009-4017.

17. Ekkad, S. V., Pamula, G., Shatiniketanam, M., “Detailed Heat Transfer Measurement Inside Straight and Tapered Two-Pass Channel with Rib Turbulators,” *Experimental Thermal and Fluid Science*, Vol. 22, 2000, pp. 155-163.

18. Murata, A., Mochizuki, S., “Effect of Rib Orientation and Channel Rotation on Turbulent Heat Transfer in a Two-Pass Square Channel with Sharp 180° Turns Investigated by Large Eddy Simulation,” *International Journal of Heat and Mass Transfer*, Vol. 47, 2004, pp. 2599-2618.

19. Chandra, P. R., Alexander, C. R., Han, J. C., “Heat Transfer and Friction Behavior in Rectangular Channel with Varying Number of Ribbed Walls,” *International Journal of Heat and Mass Transfer*, Vol. 46, 2003, pp. 481-495.

20. Webb, R. L., Eckert, E. R. G., Goldstein, R. J., “Heat Transfer and Friction in Tubes with Repeated-Rib Roughness,” *International Journal of Heat and Mass Transfer*, Vol. 14, 1971, pp. 601-617.

21. Taslim, M. E., Li, T., “Experimental Study of the Effect of Bleed Holes on Heat Transfer and Pressure Drop in Trapezoidal Passages with Tapered Turbulators,” *Journal of Turbomachinery*, Vol. 117, 1995, pp. 281-289.

APPENDIX A

Data Reduction

The mass flow rate of air through the test section is calculated as

$$\dot{m} = \frac{\pi}{4} d_o^2 CY \left[\frac{2 p_o \Delta p_o}{RT_o(1-\eta^4)} \right]^2 \quad \text{(A)}$$

Where d_o is the diameter of the orifice and is equal to 3.81 cm, Y is the expansion coefficient, C is the discharge coefficient, p_o is the pressure at the upstream of the orifice, Δp_o is the pressure drop across the orifice, R is the universal gas constant for air [287 J/Kg.K], T_o is the temperature at the orifice and η is the orifice-diameter-to-pipe-diameter ratio and is equal to 0.6.

The expansion and discharge coefficient is calculated as

$$Y = 1.0 - \frac{(0.41 + 0.35\eta^4)\Delta p_o}{1.4 p_o} \quad \text{(B)}$$

$$c = 0.5959 + 0.0312\eta^{2.1} + \frac{91.71\eta^{2.5}}{Re_{dp}^{0.75}} - 0.01584 + \frac{0.0390\eta^4}{1-\eta^4} - 0.184\eta^8 \quad \text{(C)}$$

Where, Re_{dp} is given by

$$Re_{dp} = \frac{4\dot{m}}{\pi d_p \mu} \quad \text{(D)}$$

The power input to the ith wall is given as

$$q_i = VI\left(\frac{L_i}{L_h}\right) \tag{E}$$

where, I is the current, V is the voltage across the heater, L_i is the length wall segment and L_h is the total length of the heater.

The bulk air temperature is determined as

$$T_{b,out,i} = T_{b,in,i} + \frac{q_i}{\dot{m}c_p} \tag{F}$$

Where, cp is the specific heat of air.

The starting value is the measured inlet bulk temperature and the bulk temperature at the outlet of the wall segment is calculated using the above equation. This outlet bulk temperature is taken as the inlet bulk for the subsequent wall segment.

APPENDIX B

Uncertainty Analysis

The precision index is given by

$$S_x = \sqrt{\frac{1}{N-1}\sum_{i=1}^{n}(x_i - \bar{x})^2} \qquad \text{(A)}$$

Where

$$\bar{x} = \frac{1}{N}\sum_{i=1}^{n} x_i \qquad \text{(B)}$$

The Random error is given by

$$P_x = tS_x \qquad \text{(C)}$$

The overall all uncertainty is given by

$$U_x = \sqrt{(B^2 + P_x^2)} \qquad \text{(D)}$$

Mass flow rate:

$$\dot{m} = \frac{\pi}{4} d_o^2 CY \left[\frac{2 p_o \Delta p_o}{RT_o(1-\eta^4)} \right]^2 \qquad \text{(E)}$$

$$\frac{U_{\dot{m}}}{\dot{m}} = \left[\left(\frac{1}{2}\frac{U_{p_o}}{p_o} \right)^2 + \left(\frac{1}{2}\frac{U_{\Delta p_o}}{\Delta p_o} \right)^2 + \left(\frac{-1}{2}\frac{U_{T_o}}{T_o} \right)^2 \right]^{\frac{1}{2}} \qquad \text{(F)}$$

Reynolds Number:

$$Re_{Dh} = \frac{4\dot{m}}{\mu P_w} = \frac{\dot{m}}{\mu W} \qquad \text{(G)}$$

$$\frac{U_{\mathrm{Re}_{D_h}}}{Re_{D_h}}=\left[\left(\frac{1}{2}\frac{U_{p_o}}{p_o}\right)^2+\left(\frac{1}{2}\frac{U_{\Delta p_o}}{\Delta p_o}\right)^2+\left(\frac{-1}{2}\frac{U_{T_o}}{T_o}\right)^2+\left(-\frac{U_{\mu_o}}{\mu}\right)^2+\left(-\frac{U_W}{W}\right)^2\right]^{\frac{1}{2}} \tag{H}$$

Friction Factor:

$$f=\frac{\left(\frac{\Delta p}{\Delta x}\right)D_h}{\frac{\rho\bar{u}^2}{2}}=2\rho\left(\frac{\Delta p}{\Delta x}\right)D_h\left(\frac{A_c}{\dot{m}}\right)^2 \tag{I}$$

$$\frac{U_f}{f}=\left[\left(\frac{U_\rho}{\rho_o}\right)^2+\left(\frac{U_{\Delta p}}{\Delta p}\right)^2+\left(-\frac{U_{\Delta x}}{\Delta x}\right)^2+\left(\frac{4U_W}{W}\right)^2+\left(\frac{U_W}{W}\right)^2+\left(\frac{-2U_{\dot{m}}}{\dot{m}}\right)^2\right]^{\frac{1}{2}} \tag{J}$$

Bulk Mean Temperature:

$$T_{b,out}=T_{b,in}+\frac{q}{\dot{m}c_p}=T_{b,in}+\frac{VI\left(L/L_h\right)}{\dot{m}c_p} \tag{K}$$

$$\frac{U_{T_{b,out}}}{T_{b,out}}=\left\{\begin{array}{l}\left[\left(\frac{T_{b,in}}{T_{b,outo}}\right)\left(\frac{U_{T_{b,in}}}{T_{b,in}}\right)\right]^2+\left[\left(\frac{\Delta T_b}{T_{b,outo}}\right)\left(\frac{U_V}{V}\right)\right]^2+\left[\left(\frac{\Delta T_b}{T_{b,outo}}\right)\left(\frac{U_I}{I}\right)\right]^2+\left[\left(\frac{\Delta T_b}{T_{b,outo}}\right)\left(\frac{U_L}{L}\right)\right]^2+\\ \left[\left(\frac{\Delta T_b}{T_{b,outo}}\right)\left(\frac{-U_{L_h}}{L_h}\right)\right]^2+\left[\left(\frac{\Delta T_b}{T_{b,outo}}\right)\left(\frac{-U_{\dot{m}}}{\dot{m}}\right)\right]^2+\left[\left(\frac{\Delta T_b}{T_{b,outo}}\right)\left(\frac{-U_{C_p}}{C_p}\right)\right]^2\end{array}\right\}$$

$$U_{\bar{T}_b}=U_{T_{b,in}} \tag{L}$$

Nusselt Number:

$$Nu_{D_h}=\frac{hD_h}{k}=\frac{q}{A_s(\bar{T}_W-\bar{T}_b)}\left(\frac{D_h}{k}\right)=\frac{VI\left(L/L_h\right)}{(LW)(\bar{T}_W-\bar{T}_b)}\left(\frac{W}{k}\right) \tag{M}$$

$$\frac{U_{Nu_{D_h}}}{Nu_{D_h}}=\left[\left(\frac{U_V}{V}\right)^2+\left(\frac{U_I}{I}\right)^2+\left(-\frac{U_{L_h}}{L_h}\right)^2+\left(\frac{-U_{\bar{T}_W}}{\bar{T}_W-\bar{T}_b}\right)^2+\left(\frac{U_{\bar{T}_b}}{\bar{T}_W-\bar{T}_b}\right)^2-\left(\frac{-U_k}{k}\right)^2\right]^{\frac{1}{2}} \tag{N}$$

APPENDIX C

Table 4 Properties of Air at Room Temperature

Properties	Value
Thermal conductivity [W/m K]	2.67×10^{-2}
Density [Kg/m^3]	1.181
Specific Heat at Constant Pressure [KJ/Kg]	1006
Prandtl Number	0.69
Dynamic Viscosity [Kg/ m s]	1.87×10^{-5}

APPENDIX D

Table 5 Value of t(N,C) for a Confidence Level C and Number of Degrees of Freedom υ=N-1

$\nu = N-1$	C				
	0.900	0.950	0.990	0.995	0.999
1	6.314	12.70	63.65	127.3	636.6
2	2.920	4.303	9.925	14.09	31.60
3	2.353	3.182	5.841	7.453	12.92
4	2.132	2.776	4.604	5.598	8.610
5	2.015	2.571	4.032	4.773	6.869
6	1.943	2.447	3.707	4.317	5.959
7	1.895	2.365	3.499	4.029	5.408
8	1.860	2.306	3.355	3.833	5.041
9	1.833	2.262	3.250	3.690	4.781
10	1.812	2.228	3.169	3.581	4.587
11	1.796	2.201	3.106	3.497	4.437
12	1.782	2.179	3.055	3.428	4.318
13	1.771	2.160	3.012	3.372	4.221
14	1.761	2.145	2.977	3.326	4.140
15	1.753	2.131	2.947	3.286	4.073
16	1.746	2.120	2.921	3.252	4.015
17	1.740	2.110	2.898	3.223	3.965
18	1.734	2.101	2.878	3.197	3.922
19	1.729	2.093	2.861	3.174	3.883
20	1.725	2.086	2.845	3.153	3.850
25	1.708	2.060	2.787	3.078	3.725
30	1.697	2.042	2.750	3.030	3.646
40	1.684	2.021	2.704	2.971	3.551
60	1.671	2.000	2.660	2.915	3.460
120	1.658	1.980	2.617	2.860	3.373
∞	1.645	1.960	2.576	2.807	3.291

APPENDIX E

Table 6 Tabulated Reading for Smooth Channel

	Re1=8,500	Re2=16,800	Re3=23,700	Re4=33,200	Re5=37,000
T1	324.3	320.8	321.1	322.2	322.2
T2	325.4	321.8	322.2	323.3	323.4
T3	332.7	328.4	328.9	329.6	330
T4	332.2	328	328.4	330	330.4
T5	336.2	331.4	331.7	332.6	332.8
T6	336.2	331.3	331.6	332.4	332.8
T7	339	333.9	334.1	334.7	335.3
T8	339	333.8	334	334.5	335.1
T9	341.4	336.1	336.2	336.9	337.6
T10	340.8	335.5	335.7	336.3	337
T11	0	0	0	0	0
T12	342.7	337.4	337.5	338.2	338.9
T13	341.6	336.4	336.8	337.2	338
T14	340.9	335.8	336.2	336.7	337.4
T15	336.3	332.1	333.3	332.7	333.6
T16	337.2	333.1	334.3	333.6	334.5
T17	327	323.5	323.9	324.3	324.2
T18	327.6	324.1	324.6	325.3	325.3
T19	334.3	329.8	330.2	331	331
T20	334	329.6	330	330.7	330.6
T21	338.3	333.2	333.4	334.1	334.3
T22	338.2	333.1	333.3	334	334.2
T23	0	0	0	0	0
T24	340.2	334.8	334.8	335.5	336
T25	343	337.3	337.3	338.1	338.8
T26	342.9	337.2	337.2	337.9	338.6
T27	344.2	338.3	338.3	338.9	339.6
T28	343.8	338	338	338.3	339
T29	344.4	338.9	339.3	339.4	340.4
T30	344.5	339	339.4	339.7	340.7
T31	337.6	332.9	333.5	333.4	334.5
T32	337.4	332.8	333.4	333.3	334.4
T33	327.6	324.8	325.9	325.8	325.3
T34	327.9	325	326.1	0	325.8
T35	335.5	331.7	332.8	333	332.5
T36	335.6	331.7	332.8	332.9	332.5
T37	0	0	0	0	0
T38	340.6	336.2	337.5	337.4	336.8
T39	341.8	337.3	338.6	339.1	338.7
T40	342	337.5	338.8	339.3	338.9
T41	344	339.5	340.7	341.1	340.8
T42	343.8	339.3	340.5	340.8	340.6
T43	345.2	340.7	342	341.8	341.4
T44	345.4	340.9	342.1	342	341.6
T45	345.7	341.6	343	343.9	343.2
T46	345.2	341.1	342.5	343.2	342.6
T47	340.3	336.8	338.2	339.4	338.2
T48	340	336.5	337.9	339	337.8
T49	327.2	322.9	323.4	322.1	322.8
T50	327.6	323.3	323.9	0	323.4
T51	336.1	331	332	330.9	331.9
T52	336.2	331.1	332.1	331.1	332
T53	341.4	335.8	337.1	335.8	336.9
T54	341.4	335.9	337.1	335.9	337
T55	344.4	338.6	339.9	338.5	339.7
T56	344.4	338.6	339.9	338.6	339.8
T57	346.6	340.5	341.6	340.1	341.3
T58	346.3	340.2	341.3	339.8	341
T59	347.1	341	342.1	340.5	341.7
T60	347	341	342	340.5	341.7
T61	344.9	339	339.9	338.3	339.4
T62	345.2	339.2	340.2	338.7	339.7
T63	341.9	336.8	338	336.7	337.4
T64	341.7	336.7	337.8	336.5	337.2

Power input to the straight wall					
Voltage(V)	26.171	29.153	32.19	36.44	38.166
Currrent(I)	1.409	1.577	1.74	1.96	2.062

Power input to the inclined wall					
Voltage(V)	30.778	34.806	39.41	43.9	45.71
Current(I)	1.655	1.876	2.129	2.36	2.452

Pressure upsteram of the orifice(Pressure transducer)					
Vdc(V)	0.064	0.152	0.257	0.469	0.573

Pressure drop across the test section (in of H20)					
Del p	0.002	0.003	0.006	0.007	0.009

Table 7 Tabulated Reading for Channel with 90^{o} Transverse Ribs

	Trial 1					Trial 2					Trial 3				
	Re1	Re2	Re3	Re4	Re5	Re1	Re2	Re3	Re4	Re5	Re1	Re2	Re3	Re4	Re5
(K)															
T1	324.4	320.9	321.1	323.2	323	324.8	321.6	320.9	322.9	323	325.6	321	321.6	323	322.3
T2	325.2	321.6	322.3	324.4	324.3	325.9	322.8	322	324.1	324.3	326.7	322.2	322.7	324.2	323.5
T3	330.7	326.3	326.3	328.5	328.4	330.7	327.3	326	328.2	328.4	331.8	326.9	326.8	328.2	327.5
T4	329.5	325.2	325.6	327.6	327.4	330	326.7	325.3	327.4	327.4	331	326.3	326.1	327.3	326.6
T5	330.1	325.2	325.8	327.3	327	331	328.4	325.9	327.2	327	332	328	326.7	327.3	326.6
T6	331.5	326.4	326.4	328	327.8	332	329.4	326.4	327.9	327.8	333	328.9	327.2	327.8	327.1
T7	333.1	327.7	327.7	329.5	329.2	333.8	330.7	327.7	329.4	329.2	334.8	330.2	328.7	329.3	328.5
T8	333.4	328	328	329.8	329.5	334	330.5	328	329.6	329.5	335.1	330	328.9	329.6	328.7
T9	334.4	328.7	328.7	330.4	330.1	335.3	332.6	328.8	330.2	330.1	336.3	332.2	329.8	330.1	329.3
T10	334	328.4	328.3	330	329.6	334.8	332.4	328.4	329.8	329.6	335.8	331.9	329.3	329.7	328.9
T11	0	0	0	0	0	0	0	0	0	0	0	0	0	0	0
T12	335.1	329.5	329.9	331.7	331.3	336.5	333.5	329.9	331.4	331.3	337.5	333	330.8	331.3	330.5
T13	334.2	328.6	328.9	330.5	330.2	335.5	332.5	329	330.3	330.2	336.5	331.9	329.8	330.2	329.3
T14	334	328.5	328.4	330	329.7	335	331.9	328.5	329.8	329.7	335.9	331.4	329.4	329.7	328.9
T15	330	325	324.6	325.8	325.2	330.9	329.1	325	325.6	325.2	331.5	328.5	325.9	325.6	324.6
T16	330.6	325.7	325.2	326.5	326	331.4	329.3	325.5	326.3	326	332	328.7	326.4	326.3	325.4
T17	326.8	322.8	323	325.2	324.7	326.9	322.4	322.3	324.7	324.7	327.8	321.9	323.6	325.1	323.7
T18	327.3	323.2	323.5	325.7	325.4	327.5	322.9	322.9	325.3	325.4	328.5	322.3	324.1	325.8	324.5
T19	330.9	326	325.8	327.9	327.4	331.3	325	325.6	327.8	327.4	332.4	324.6	327.2	328.4	326.9
T20	330.6	325.7	325.9	327.9	327.5	331.2	325.1	325.5	327.8	327.5	332.4	324.7	327.1	328.4	326.8
T21	332.5	326.5	326.4	328.3	327.9	332.9	326.9	326.4	328.3	327.9	334.1	326.8	328	328.9	327.3
T22	332.3	326.5	326.3	328.1	327.7	332.8	327	326.2	328.1	327.7	334	326.7	327.9	328.7	327.1
T23	0	0	0	0	0	0	0	0	0	0	0	0	0	0	0
T24	332.8	327.1	326.7	328.5	328	333.5	327.6	326.6	328.5	328	334.7	327	328.3	329	327.3
T25	334.8	328.6	328.3	330.3	329.8	335.8	328.9	328.3	330.2	329.8	337	328.3	330	330.7	329.1
T26	334.8	328.7	328.2	330.1	329.6	335.6	328.9	328.2	330.1	329.6	336.8	328.3	329.9	330.5	329
T27	335.8	329.6	329.3	331.2	330.8	336.9	329.7	329.3	331.2	330.8	338.1	329.1	330.9	331.5	330
T28	335.4	329.3	329	331	330.5	336.5	329.6	328.9	330.9	330.5	337.7	329.1	330.6	331.3	329.7
T29	336.8	330.9	330.6	332.7	332.3	337.7	331.1	330.4	332.6	332.3	338.9	330.6	331.9	332.8	331.4
T30	337.1	331.2	331	333.1	332.6	338	331.2	330.7	332.9	332.6	339.2	330.7	332.3	333.2	331.8
T31	330.8	325.3	324.6	325.9	325.3	331.8	326	325	325.9	325.3	332.7	325.4	326.4	326.3	324.7
T32	330.4	324.8	324.6	325.8	325.1	331.8	325.9	325.1	325.8	325.1	332.7	325.2	326.4	326.2	324.6
T33	326.2	323.7	322.7	325.6	325.6	328	322.8	324.1	326.1	325.6	329.5	324.9	323.4	326.9	325.9
T34	326.7	323.6	323.1	0	326.2	328.4	323.3	324.4	0	326.2	329.9	325.3	323.9	0	326.4
T35	331.7	328	326.9	329.8	329.9	333.6	327.2	328.3	330.4	329.9	335.5	329.5	327.6	331.2	330
T36	331.8	328.1	326.9	329.8	329.8	333.7	327.3	328.4	330.3	329.8	335.6	329.6	327.6	331.2	330
T37	0	0	0	0	0	0	0	0	0	0	0	0	0	0	0
T38	334.9	330.6	329.1	331.8	331.7	337	329.5	330.6	332.4	331.7	339.1	332.1	329.7	333.3	331.9
T39	335.5	331.1	329.4	332.2	332.1	337.8	329.8	331	332.8	332.1	340	332.5	330	333.7	332.4
T40	335.7	331.3	329.7	332.5	332.4	338	330	331.3	333.1	332.4	340.2	332.8	330.3	334	332.7
T41	336.7	332	330.1	332.7	332.6	339.1	330.6	331.7	333.3	332.6	341.4	333.4	330.7	334.3	332.9
T42	336.5	331.8	329.9	332.5	332.4	338.9	330.4	331.6	333.2	332.4	341.3	333.2	330.6	334.1	332.8
T43	337.4	332.6	330.4	332.5	332.3	340	331.1	332.1	333.2	332.3	342.4	334	331.1	334.2	332.6
T44	337.6	332.8	330.6	332.8	332.6	340.2	331.3	332.3	333.4	332.6	342.6	334.2	331.3	334.5	332.9
T45	338.7	334.5	332.7	335.6	335.6	341.2	332.9	334.4	336.2	335.6	343.7	335.8	333.3	337.2	335.8
T46	338.2	334.1	332.3	335.3	335.2	340.8	332.5	334	335.8	335.2	343.3	335.4	332.9	336.8	335.4
T47	333.5	330.1	328.5	331.3	331.2	335.8	328.5	330	331.7	331.2	337.9	331.2	328.9	332.6	331.4
T48	333.2	329.8	328	330.8	330.6	335.4	328.1	329.7	331.3	330.6	337.5	330.9	328.5	332.2	330.8
T49	322.8	319.1	318.2	320.1	320	324.7	319.2	319.6	320.6	320	325.7	320.7	319	321.5	320.2
T50	323.2	319.4	318.7	0	320.5	325.1	319.5	320	0	320.5	326.1	321.1	319.5	0	320.7
T51	329.1	324.7	323.7	326.3	326.3	331.4	324.6	325.4	326.9	326.3	332.8	326.4	324.7	327.9	326.5
T52	329.2	324.8	324	326.6	326.6	331.5	324.7	325.5	327.2	326.6	332.9	326.6	324.9	328.2	326.8
T53	332.5	327.5	326.4	329.3	329.4	334.9	327.2	328.1	329.9	329.4	336.6	329.2	327.3	330.9	329.4
T54	332.6	327.6	326.5	329.4	329.6	335	327.3	328.2	330.1	329.6	336.7	329.4	327.4	331	329.6
T55	334.4	329.3	328	330.9	331	336.9	328.7	329.7	331.6	331	338.7	330.9	328.8	332.5	331
T56	334.4	329.4	328.1	331.1	331.2	337	328.8	329.9	331.8	331.2	338.8	331	329	332.8	331.3
T57	335.8	330.4	328.8	331.6	331.7	338.4	329.6	330.7	332.4	331.7	340.4	332	329.7	333.3	331.7
T58	335.6	330.3	328.8	331.6	331.6	338.3	329.5	330.7	332.3	331.6	340.3	331.9	329.7	333.3	331.7
T59	336.7	331.6	330	333.1	333.2	339.4	330.6	331.9	333.9	333.2	341.5	333.1	330.9	334.8	333.3
T60	336.6	331.6	330	333.2	333.2	339.3	330.6	332	333.9	333.2	341.5	333.1	331	334.9	333.3
T61	334.2	328.9	327.2	329.8	329.7	336.8	327.9	329.1	330.4	329.7	338.9	330.4	328.1	331.4	329.8
T62	334.5	329.2	327.5	330.1	330	337.1	328.3	329.4	330.7	330	339.2	330.8	328.4	331.7	330.2
T63	332.1	327.7	326.3	329.1	329.1	334.6	326.8	328.1	329.6	329.1	336.3	329.1	327.1	330.6	329.2
T64	332	327.5	326.2	328.9	328.9	334.4	326.6	328	329.4	328.9	336.1	329	327	330.5	329
						Power input to the straight wall									
Voltage(V)	32.23	36.05	39.92	45.81	47.62	32.03	36.046	39.92	45.69	47.62	32.06	36	40.01	45.9	47.37
Currrent(I)	1.75	1.92	2.06	2.42	2.53	1.7	1.92	2.06	2.417	2.517	1.71	1.91	2.064	2.39	2.47
						Power input to the inclined wall									
Voltage(V)	38.06	42.9	47.03	54.66	57.25	38.11	42.89	46.95	54.66	56.88	38.23	42.87	47.03	54.66	56.89
Current(I)	2.06	2.28	2.47	2.89	3.02	2.02	2.28	2.47	2.89	3.02	2.03	2.26	2.468	2.89	3.02
						Pressure upsteram of the orifice(Pressure transducer)									
Vdc(V)	0.07	0.173	0.299	0.551	0.674	0.07	0.173	0.299	0.551	0.674	0.07	0.173	0.299	0.551	0.674
						Pressure drop across the test section (in of H20)									
Del p	0.003	0.006	0.03	0.097	0.153	0.003	0.006	0.03	0.097	0.153	0.003	0.006	0.03	0.097	0.153

Table 8 Tabulated Reading for Channel with 45° V-shaped Ribs

	Trial 1					Trial 2					Trial 3				
	Re1	Re2	Re3	Re4	Re5	Re1	Re2	Re3	Re4	Re5	Re1	Re2	Re3	Re4	Re5
(K)															
T1	326.3	322.1	321.1	323.9	323.7	326.8	321.6	320.9	324.2	323.5	327	321	320.8	324.2	323.7
T2	327.4	323.4	322.4	325.6	325.4	327.9	322.8	322.3	325.9	325.2	328.1	322.2	322.2	325.9	325.4
T3	333.4	328	326.6	330.3	329.8	333.8	327.3	326.6	330.5	329.6	334	326.9	326.5	330.5	329.8
T4	332.6	327.4	326.1	329.7	329.2	333	326.7	326	329.9	329.1	333.1	326.3	326	329.9	329.2
T5	334.9	329.2	327.6	331.2	330.6	335.5	328.4	327.6	331.5	330.6	335.7	328	327.4	331.5	330.6
T6	336.1	330.2	328.6	332.3	331.6	336.7	329.4	328.6	332.5	331.6	336.9	328.9	328.3	332.5	331.6
T7	338	331.5	329.7	333.5	332.6	338.7	330.7	329.7	333.7	332.6	338.8	330.2	329.4	333.7	332.6
T8	337.6	331.2	329.4	333.2	332.5	338.4	330.5	329.5	333.5	332.4	338.5	330	329.2	333.5	332.5
T9	340.5	333.4	331.3	335.5	334.9	341.2	332.6	331.7	335.9	334.8	341.3	332.2	331.2	335.9	334.9
T10	340.2	333.2	331.1	335.4	334.7	340.9	332.4	331.5	335.7	334.6	341	331.9	330.9	335.7	334.7
T11	0	0	0	0	0	0	0	0	0	0	0	0	0	0	0
T12	341.7	334.3	331.9	336.6	336.1	342.3	333.5	332.8	337.1	336	342.4	333	332	337.1	336.1
T13	340.6	333.3	330.8	335.1	334.6	341.1	332.5	331.7	335.7	334.6	341.3	331.9	330.8	335.7	334.6
T14	339.9	332.8	330.3	334.6	334.1	340.3	331.9	331.1	335.2	334.2	340.5	331.4	330.3	335.2	334.1
T15	336.1	329.9	327.7	331.3	330.9	336.8	329.1	328.2	331.8	331	336.9	328.5	327.5	331.8	330.9
T16	336.4	330.1	327.9	331.6	331.1	336.9	329.3	328.4	332.1	331.2	337	328.7	327.7	332.1	331.1
T17	327.2	323	321.9	325	324.8	327.7	322.4	321.7	325.2	324.4	327.9	321.9	321.7	325.2	324.8
T18	327.6	323.4	322.4	325.7	325.5	328.1	322.9	322.2	325.9	325.1	328.4	322.3	322.3	325.9	325.5
T19	331.5	325.7	323.6	326.2	325.6	332	325	323.7	326.5	325.4	332.4	324.6	323.6	326.5	325.6
T20	331.6	325.8	323.7	326.5	326	332	325.1	323.9	326.8	325.8	332.4	324.7	323.7	326.8	326
T21	334.9	326.9	326.3	329.7	328.8	334.9	326.9	326.3	329.7	328.7	335.2	326.8	325.8	329.7	328.8
T22	334.8	327	326.3	329.7	328.8	334.8	327	326.3	329.7	328.7	335.2	326.7	325.8	329.7	328.8
T23	0	0	0	0	0	0	0	0	0	0	0	0	0	0	0
T24	335.3	328.3	325.8	329.2	328.8	335.8	327.6	326.5	329.7	328.8	336	327	325.8	329.7	328.8
T25	337.2	329.5	327	330.7	330.2	337.6	328.9	327.9	331.2	330.3	337.8	328.3	327.1	331.2	330.2
T26	337.2	329.5	327	330.8	330.4	337.6	328.9	327.9	331.3	330.4	337.8	328.3	327.1	331.3	330.4
T27	338.3	330.4	327.7	331.5	331	338.6	329.7	328.7	332	331	338.9	329.1	327.8	332	331
T28	338.1	330.3	327.7	331.5	331	338.4	329.6	328.6	332.1	331.1	338.6	329.1	327.8	332.1	331
T29	339.3	331.9	329.6	333.8	333.3	339.6	331.1	330.1	334.3	333.3	339.9	330.6	329.7	334.3	333.3
T30	339.6	332.1	329.8	334.1	333.4	339.9	331.2	330.3	334.5	333.5	340.2	330.7	329.8	334.5	333.4
T31	333.5	326.7	324.4	327	326	334	326	324.6	327.4	326.4	334.1	325.4	324.1	327.4	326
T32	333.4	326.5	324.2	326.6	325.5	334	325.9	324.3	326.9	325.9	334.1	325.2	323.9	326.9	325.5
T33	329.2	324.1	323.2	326	325.5	329.5	323.6	323.5	326.5	325.6	329.6	322.7	323.2	326.3	325.5
T34	329.7	324.5	323.7	0	326.1	330	324.1	324	0	326.1	330	323.2	323.7	0	326.1
T35	335.7	329.1	328	331.9	331.2	335.7	328.5	328.7	332.4	331.4	335.7	327.5	327.9	332	331.2
T36	335.8	329.3	328.2	332.2	331.6	335.9	328.7	328.9	332.7	331.7	335.8	327.6	328.1	332.3	331.6
T37	0	0	0	0	0	0	0	0	0	0	0	0	0	0	0
T38	338.6	331.2	329.8	334	333.2	338.5	330.5	330.6	334.5	333.4	338.4	329.4	329.7	334	333.2
T39	339	331.5	330.1	334.1	333.3	338.9	330.7	330.7	334.6	333.6	338.9	329.7	329.8	334.1	333.3
T40	339.2	331.7	330.3	334.4	333.5	339.1	331	330.9	334.9	333.8	339.1	329.9	330.1	334.3	333.5
T41	340.5	332.6	331	334.9	334	340.5	331.8	331.6	335.5	334.4	340.3	330.7	330.8	334.9	334
T42	340.3	332.4	330.8	334.7	333.8	340.3	331.6	331.4	335.2	334.1	340.2	330.5	330.6	334.7	333.8
T43	341.9	333.9	332.5	336.4	335.2	342.1	333.1	332.9	336.8	335.6	341.9	332	332.2	336.3	335.2
T44	342	334	332.5	336.5	335.3	342.2	333.2	332.9	336.9	335.7	342	332.1	332.3	336.4	335.3
T45	343.2	335.1	333.9	337.4	336.1	343.6	334.3	333.8	337.8	336.5	343.3	333.2	333.4	337.3	336.1
T46	342.6	334.6	333.4	337	335.7	343.1	333.9	333.4	337.4	336.1	342.9	332.8	333	336.9	335.7
T47	338.1	331.4	330.6	334.3	333.2	338.8	330.6	330.4	334.7	333.7	338.4	329.6	330.1	334.1	333.2
T48	337.5	330.8	330	333.5	332.5	338.2	330	329.8	333.8	332.9	337.9	329.1	329.6	333.4	332.5
T49	326.8	321.9	321.4	323.9	323.2	327.2	321.5	321.4	324.2	323.4	327.1	320.6	321.1	323.9	323.2
T50	327.2	322.3	321.8	0	323.8	327.6	322	321.8	0	324	327.5	321	321.6	0	323.8
T51	333.5	327.3	326.6	330.3	329.5	333.7	326.9	327	330.7	329.8	333.5	325.7	326.3	330.1	329.5
T52	333.6	327.4	326.7	330.5	329.6	333.8	327	327.2	330.9	330	333.6	325.8	326.4	330.3	329.6
T53	336.3	329.1	327.9	332.1	331.3	336.3	328.7	329	332.7	331.8	336.1	327.4	327.8	331.8	331.3
T54	336.3	329.2	327.9	332.1	331.3	336.3	328.8	329	332.7	331.8	336.1	327.4	327.8	331.8	331.3
T55	338.1	331.2	330.1	335	334.2	337.8	330.7	331.3	335.6	334.8	337.6	329.3	329.9	334.6	334.2
T56	338.1	331.2	330.2	335.3	334.4	337.8	330.7	331.4	335.7	335	337.6	329.3	330	334.8	334.4
T57	339.2	331.6	330.5	335.3	334.2	338.9	331.1	331.5	335.7	335	338.7	329.8	330.3	334.7	334.2
T58	338.7	331.3	330.2	334.8	333.9	338.4	330.8	331.1	335.4	334.7	338.2	329.4	329.9	334.3	333.9
T59	339.3	331.8	330.9	335.3	334.2	339.3	331.4	331.6	335.7	335	339.1	330.2	330.6	334.8	334.2
T60	339.4	331.9	331	335.5	334.3	339.3	331.5	331.6	335.9	335.1	339.1	330.2	330.7	334.9	334.3
T61	337.7	330	329	332.5	331.4	338	329.5	329.1	332.9	332.1	337.7	328.4	328.7	332.2	331.4
T62	338	330.3	329.3	332.9	331.7	338.3	329.8	329.4	333.2	332.4	338	328.6	329	332.5	331.7
T63	335.7	329.3	329.1	333	331.9	336.4	328.9	328.9	333.3	332.6	335.9	327.8	328.8	332.7	331.9
T64	335.7	329.2	329.1	333	331.9	336.4	328.8	328.9	333.3	332.5	335.9	327.7	328.8	332.7	331.9
Power input to the straight wall															
Voltage(V)	33.3	37.5	41.9	49.82	50.62	33.42	37.37	42.02	49.63	50.62	33.45	37.46	41.55	49.85	50.67
Currrent(I)	1.78	2	2.22	2.64	2.66	1.78	1.99	2.2	2.62	2.67	1.78	1.98	2.185	2.65	2.68
Power input to the inclined wall															
Voltage(V)	40.2	44.4	49.96	59.18	60.04	40.33	44.57	50.04	59	59.97	40.26	44.13	49.64	59.36	59.88
Current(I)	2.18	2.35	2.66	3.13	3.19	2.13	2.35	2.65	3.18	3.21	2.13	2.29	2.61	3.15	3.17
Pressure upsteram of the orifice(Pressure transducer)															
Vdc(V)	0.069	0.179	0.314	0.574	0.713	0.069	0.179	0.314	0.574	0.713	0.069	0.179	0.314	0.574	0.713
Pressure drop across the test section (in of H20)															
Del p	0.006	0.025	0.049	0.09	0.117	0.006	0.025	0.049	0.09	0.117	0.006	0.025	0.049	0.09	0.117

VITA

Name:	Karthik Subramanian
Address:	c/o Dr. Sai C.Lau Department of Mechanical Engineering Texas A&M University College Station, Texas 77843-3123
Email Address:	karthik_30182@tamu.edu
Education:	B.E., Mechanical Engineering, University of Madras, 2003 M.S., Mechanical Engineering, Texas A&M University, 2005